Journal of Structural Geology 32 (2010) 920–940

Contents lists available at ScienceDirect

Journal of Structural Geology

journal homepage: www.elsevier.com/locate/jsg

Deformation temperatures, vorticity of flow, and strain in the Moine thrust zone and Moine nappe: Reassessing the tectonic evolution of the Scandian foreland–hinterland transition zone

J. Ryan Thigpen [a,*], Richard D. Law [a], Geoffrey E. Lloyd [b], Summer J. Brown [a]

[a] Department of Geosciences, Virginia Tech, 4044 Derring Hall, Blacksburg, VA 24061, USA
[b] School of Earth and Environment, The University, Leeds LS2 9JT, UK

ARTICLE INFO

Article history:
Received 18 May 2009
Received in revised form
21 April 2010
Accepted 2 May 2010
Available online 10 May 2010

Keywords:
Moine
Scotland
Vorticity
Strain
Assynt
Deformation temperatures

ABSTRACT

Examination of deformation temperature, 3-D strain and flow vorticity (W_m) in mylonites from the Assynt-Loch More region of the Moine thrust zone (MTZ) allows quantitative kinematic and thermal characterization of shearing at the base of the Scandian (435–425 Ma) orogenic wedge. Quartz microstructures and c-axis fabric opening angles from mylonites in the immediate hangingwall and footwall to the Moine thrust suggest that deformation temperatures are highest in the eastern part of the Assynt region (including mylonites close to alkaline intrusive complexes) and decrease along strike both to the north (Stack of Glencoul – Loch More) and to the south (Knockan). Quartz c- and a-axis fabrics, together with limited 3-D strain data, indicate that deformation in both the footwall and hangingwall mylonites dominantly involved plane strain to general flattening, although domains of more constrictional flow are identified adjacent to thrust transport-parallel lineaments in the overlying Moine nappe. Rigid grain analyses indicate a remarkably constant flow vorticity for tens of kilometers along orogenic strike (40–60% pure shear) in both the hangingwall and footwall mylonites. Integration with previously reported strain and vorticity estimates from the Assynt region indicates a 50–75% sub-vertical shortening perpendicular to gently dipping foliation, that must have been accommodated by either volume loss or extrusion of material toward the synorogenic topographic surface. Extrusion implies a causal link between upper and lower crustal processes, with significant implications for the kinematic and geometric evolution of the Scandian wedge.

1. Introduction

Recent integration of vorticity and strain studies indicates that ductile deformation in the hinterland regions of collisional orogenic systems (High Himalaya, Scottish Caledonides, European Alps, Greek Hellenides, Appalachian Blue Ridge) involves a significant component of pure shear deformation (Kassem and Ring, 2004; Law et al., 2004; Jessup et al., 2006; Bailey et al., 2007; Larson and Godin, 2009; Law, 2010; Thigpen et al., 2010; Xypolias et al., 2010). Kinematic and mechanical models that attempt to explain thrust kinematics and wedge dynamics (Chapple, 1978; Davis et al., 1983; Dahlen et al., 1984; Platt, 1986; Dahlen, 1990; Holdsworth and Grant, 1990; Willett et al., 1993) must take these pure shear components into account. Major theoretical implications of a significant pure shear contribution to ductile deformation include: 1) vertical ductile thinning contributes to synkinematic exhumation of progressively lower portions of the orogenic wedge (Feehan and Brandon, 1999); 2) under approximately plane strain isochoric conditions, vertical ductile thinning leads to significant transport-parallel lengthening of thrust sheets, driving ductile extrusion toward the synorogenic topographic surface. In the former case, vertical ductile thinning acting in conjunction with erosion and normal faulting generates rapid synkinematic exhumation which may, in turn, explain preservation of inverted metamorphic isograds observed in the structurally lower levels of many orogenic wedges (e.g. Stephenson et al., 2000; Vannay and Grasemann, 2001; Kidder and Ducea, 2006) by vertical ductile thinning of the overlying nappe pile (Ring and Kassem, 2007). Ductile extrusion toward the synorogenic topographic surface has kinematic, geometric, and strain rate implications for deformation occurring at upper crustal levels (Williams and Jiang, 2006) and may result in kinematic and dynamic linkage between lower crustal ductile processes and upper crustal brittle processes (Northrup, 1996).

The majority of previously published vorticity studies have focused on identifying variation in vorticity and 3-D strain with change in structural depth along orogen normal sampling

* Corresponding author. Tel.: +1 5402319740; fax: +1 5402313386.
E-mail address: thigpe05@vt.edu (J.R. Thigpen).

0191-8141/$ – see front matter © 2010 Elsevier Ltd. All rights reserved.
doi:10.1016/j.jsg.2010.05.001

transects. Many of these studies have almost exclusively related vorticity variation to either structural position or to rheologic partitioning controlled by lithologic variation (e.g. Sullivan, 2008). However no studies have, to date, examined whether significant variation of flow vorticity occurs along orogenic strike. In this paper we first present new vorticity and deformation temperature data obtained from Moine thrust zone (MTZ) samples collected along strike at the base of the Scandian orogenic wedge exposed in northwest Scotland (Fig. 1). The sampling traverse is approximately 30 km in length and extends from Loch Dionard southwards through the eastern part of the Assynt district to Knockan (Fig. 2). A complementary quartz petrofabric study allows the plane strain vs. non-plane strain and coaxial vs. non-coaxial components of the deformation to be qualitatively characterized. We then discuss the tectonic significance of a pure shear contribution to ductile flow, as well as the factors that may influence variation in flow both along and across orogenic strike. Variation in estimated flow vorticities is examined with respect to lithology, deformation temperature, 3-D strain type and structural position within the nappe stack, as well as with respect to footwall structural architecture.

2. Tectonic setting

The Scandian orogenic wedge exposed in northwest Scotland (Fig. 1) is the composite result of at least three structural-thermal events, including the Knoydartian thermal event (820–730 Ma) and the Grampian (475–460 Ma) and Scandian (435–415 Ma) phases of

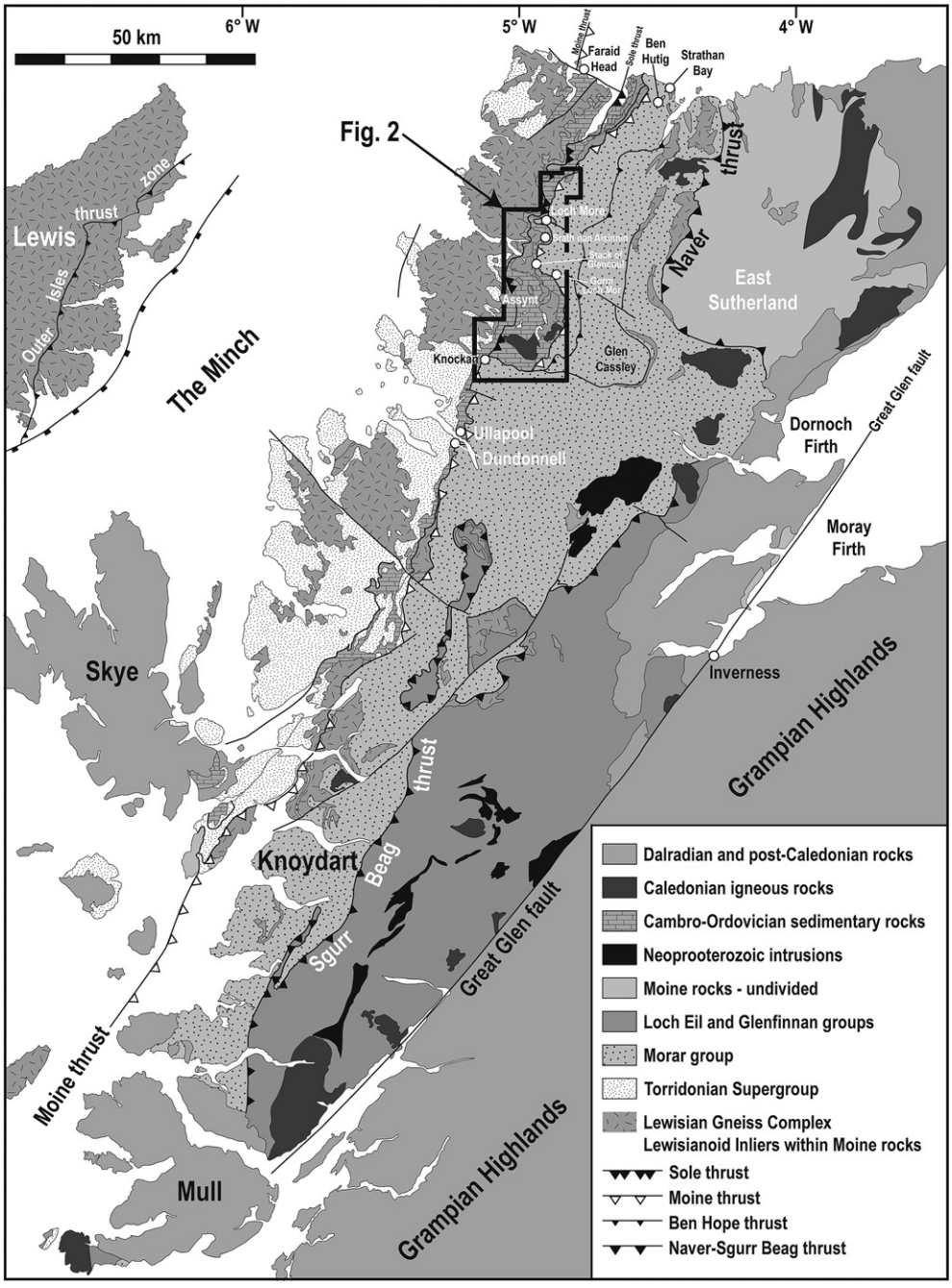

Fig. 1. Geologic map of northern Scotland. Location of Fig. 2a is shown. Modified from Krabbendam et al. (2008).

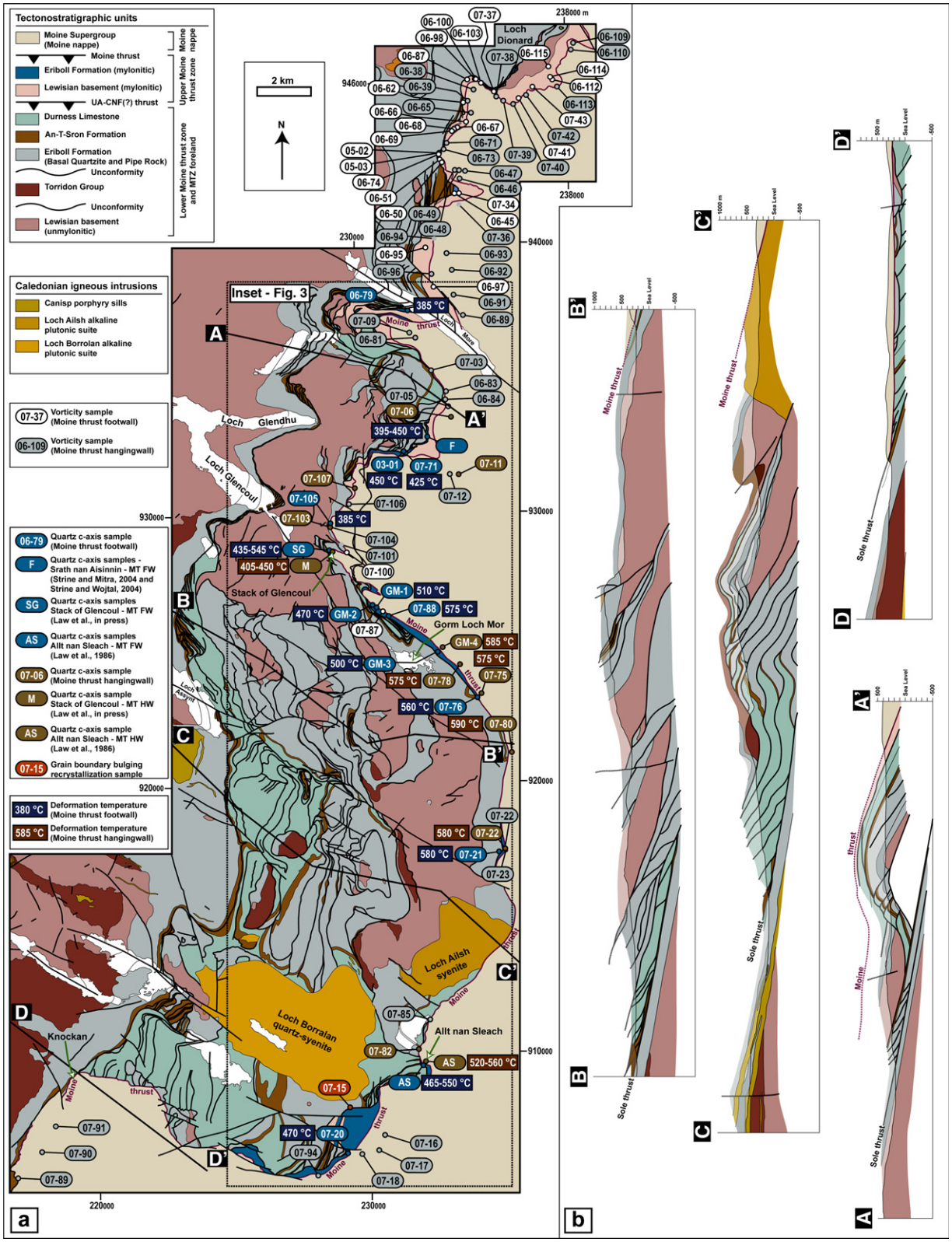

Fig. 2. (a) Detailed geologic map of the study area, showing location of samples collected for vorticity and strain symmetry analyses and for quartz petrofabrics/deformation temperature estimates. Modified after Cheer (2006) and British Geological Survey (2007). (b) Cross-sections of the Assynt region. Modified from British Geological Survey (2007). Location of section lines shown on Fig. 2a. Note that scale of sections is 2× that of map scale to show greater detail. No vertical exaggeration.

the Caledonian orogeny. The mid-Neoproterozoic Knoydartian structural-thermal event is interpreted to result from crustal thickening, possibly preceded by extension (Vance et al., 1998; Cutts et al., 2009). Grampian orogenesis, which is attributed to an arc-continent collision, resulted in significant crustal thickening (<35 km; Friend et al., 2000). Later Scandian thrusting and associated penetrative deformation produced the present structural architecture. From west to east, three major ductile thrust sheets (Moine, Naver, Skinsdale) are variably deformed and metamorphosed and internally imbricated by Scandian ductile thrusts (Fig. 1; Holdsworth et al., 2001; Strachan et al., 2002). At the base of the ductile Scandian orogenic wedge, mylonites along the upper part of the MTZ represent the foreland to hinterland transition zone of the Scottish Caledonides. Structurally beneath the upper MTZ mylonites, numerous major and minor thrusts of the lower MTZ imbricate zone accommodate west-northwest directed brittle thrusting and folding of Archaean (Lewisian) basement and overlying Neoproterozoic (Torridonian) and Cambrian platform successions (Fig. 2).

3. Structural geometry of the Moine thrust zone and Moine nappe

The MTZ, which accommodates Scandian (435–420 Ma) convergence and shortening along numerous thrusts that become progressively more brittle to the west, can be subdivided into two major components; the lower and upper MTZ, respectively. In the Assynt district, the lower MTZ is 10–15 km wide and contains the Sole, Glencoul and Ben More thrusts (Fig. 2; Peach et al., 1888, 1907) that accommodate brittle thrusting and folding between the Scandian foreland and the upper MTZ ductile thrusts. The Sole thrust (Fig. 2) represents the structurally lower limit of major Scandian deformation (Knipe, 1990; Mendum et al., 2009). The Sole and related thrusts are overlain by the Glencoul (20–25 km displacement) and Ben More (~28 km displacement) thrust sheets, and their associated smaller thrusts and duplexes (Peach et al., 1888, 1907; Elliott and Johnson, 1980; Fig. 2a).

Along strike to the north of Assynt, the upper MTZ mylonites are floored by the Upper Arnaboll-Creag na Faoilin (UA-CNF) thrust in the southern part of the Eriboll region (Holdsworth et al., 2006, 2007; Thigpen, 2009) and the Arnaboll thrust in northern Eriboll (British Geological Survey, 2002). Although currently controversial, we suggest that the UA-CNF thrust sheet (or its lateral equivalent {s}) may extend southward along strike from Eriboll through the Loch More area into the eastern part of the Assynt district. Traced up structural section toward the east, this structure marks the first major appearance of mylonitic rocks that experienced pervasive deformation at mid-crustal conditions (Dayan, 1981; Thigpen, 2009; Thigpen et al., 2010). As such it is generally interpreted to represent the foreland–hinterland transition zone in this region (Thigpen, 2009). In the Assynt district, the lateral equivalent of the UA-CNF thrust emplaces mylonitic Lewisian basement gneiss and Cambrian quartzite above the lower MTZ (Fig. 2). To the east and structurally above this mylonitic thrust sheet(s), the Moine thrust (roof thrust of the upper MTZ) emplaces mylonitic Lewisianoid basement gneiss and Moine Supergroup psammite and pelite over the transitional ductile to brittle thrusts cropping out to the west. The Ben Hope and related ductile thrusts internally imbricate the overlying Moine nappe (Holdsworth and Grant, 1990; British Geological Survey, 2002, 2009; Cheer, 2006; Leslie et al., 2010).

3.1. Relationships between mylonitic thrust sheet(s) and Moine nappe in the Assynt region

South of the Stack of Glencoul (Fig. 2a), ductile high-strain mylonites (derived from Cambrian quartzite) are only preserved as discontinuous lenses in the footwall to the Moine thrust, where they are juxtaposed between high strain rocks of the overlying Moine nappe and low penetrative strain rocks of the underlying lower MTZ, which exhibit transitional brittle to low temperature ductile deformation features (see reviews by Knipe, 1990; Law and Johnson, 2010). The contact between the mylonites and underlying low strain rocks is not exposed, but is presumably marked by an un-named thrust (Fig. 3). We interpret the lenses of mylonite, where present, to represent fragments of the UA-CNF thrust sheet recognized in the Eriboll area to the north. Where mylonites are absent in the footwall to the Moine thrust, the structure mapped as the Moine thrust (Geological Survey of Great Britain, 1923; British Geological Survey, 2007) locally emplaces ductilely deformed rocks of the Moine nappe directly on top of lower MTZ rocks that exhibit little or no penetrative deformation. Because this junction represents a contact between non-mylonitic lower MTZ rocks and overlying mylonitic rocks of the upper MTZ and Moine nappe, it must have developed as a brittle structure, at least at structurally higher levels toward the foreland. This structural contact could represent a late brittle fault cutting across the original ductile Moine thrust, which in the Assynt area, places mylonitic rocks of the Moine nappe on mylonitic Cambrian quartzite of the underlying MTZ (see Law et al., 1986, their Figs. 3 and 13), and locally cutting out the ductile Moine thrust mylonites. Microstructural analysis indicates a greater contrast in inferred temperatures associated with penetrative deformation between the mylonites in the footwall to the ductile Moine thrust (UA-CNF thrust sheet) and the underlying low strain rocks of the thrust belt than between these mylonites and the overlying high strain rocks of the Moine nappe (Thigpen, 2009). This relationship could indicate that either total displacement on the un-named thrust at the base of the mylonites is greater than on the older overlying ductile Moine thrust, or that the un-named thrust has more of a ramp-like geometry with respect to isotherms, while the ductile Moine thrust was oriented at a lower angle to isotherms (i.e. thrust flat).

3.2. Constraints on timing of Scandian deformation and thrusting in the Assynt district

Timing of thrusting is constrained by field relationships between major brittle thrusts and alkaline intrusions located both within the thrust belt and in the foreland (Fig. 2). The Canisp Porphyry sills located beneath the Sole thrust are thought to predate thrusting and have been dated at 437 ± 4.8 Ma (U–Pb TIMS zircon; Goodenough et al., 2006). The Loch Borrolan syenite, which lies below the Ben More thrust, has a U–Pb zircon crystallization age of 430 ± 4 Ma (van Breemen et al., 1979). Whilst field relationships between the Loch Borrolan intrusion and the surrounding thrusts remain controversial (see Searle et al., 2010), pervasively deformed pseudoleucites in the eastern part of the Borrolan complex (Bailey and McCallien, 1934) resulted from solid-state deformation associated with thrusting following crystallization, but prior to final cooling of the intrusion. The Loch Ailsh intrusive complex, located between the Ben More and Moine thrusts, was originally dated at 439 ± 4 Ma (Halliday et al., 1987; U–Pb zircon crystallization age), but has recently been re-dated by the British Geological Survey at 430.6 ± 0.3 Ma (Kathryn Goodenough, pers. comm. 2010). Although the contacts are not exposed, the Loch Ailsh complex may be cut by both the Ben More and Moine thrusts, and therefore crystallization should predate thrusting in the MTZ. Structurally above the MTZ, Rb–Sr white mica crystallization ages of 437–408 Ma were obtained from Moine mylonites at Knockan (southern Assynt; Fig. 2) and in the Dundonnell area to the south of Assynt (Fig. 1; Freeman et al., 1998). Rb–Sr muscovite cooling ages (closure $T \sim 550\ ^{\circ}C$) of c. 428 Ma, c. 421 Ma, and c. 413 Ma were obtained from mylonites in the

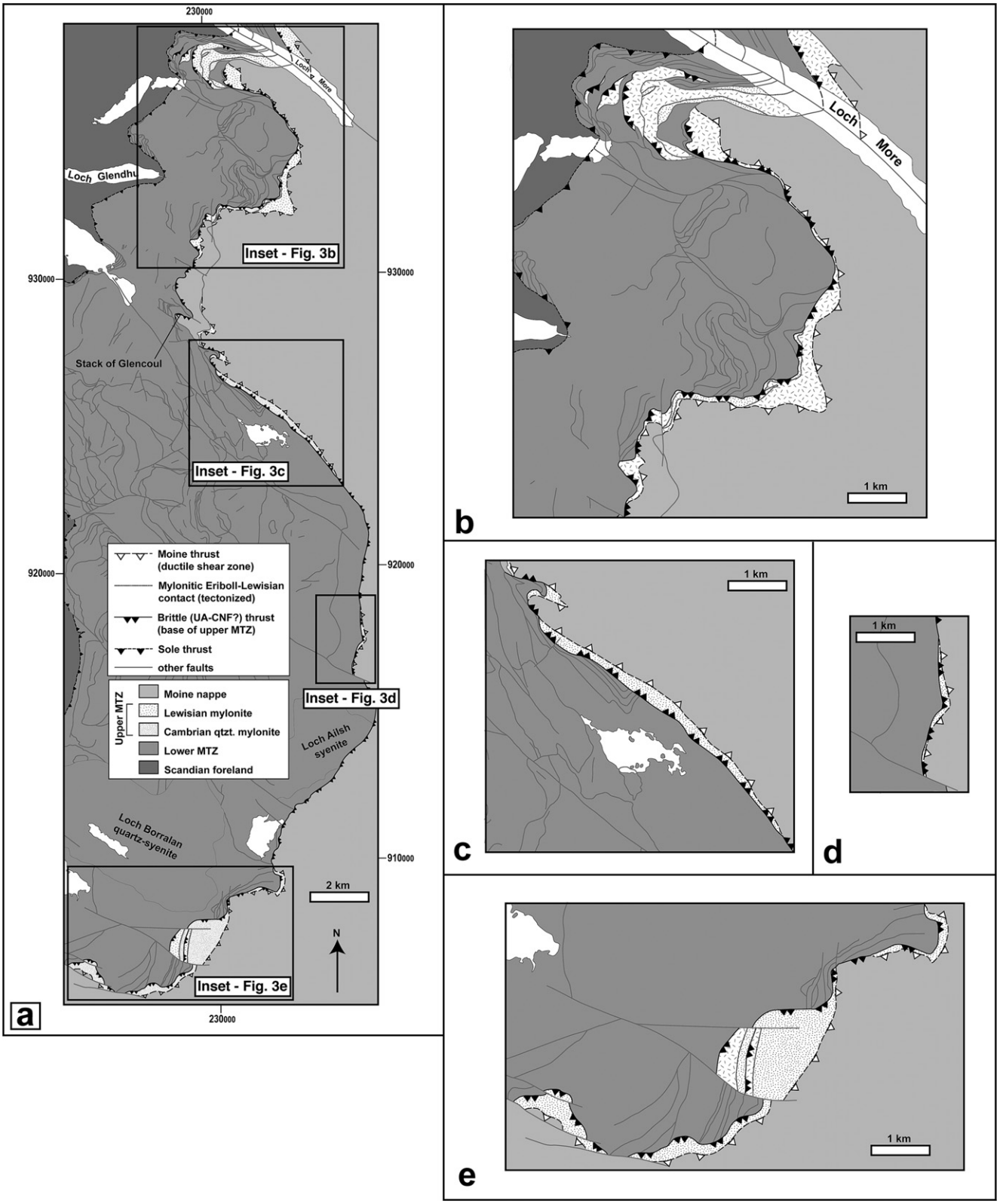

Fig. 3. Simplified geologic map of (a) the eastern part of the Assynt region and detailed inset maps of: (b) northern Assynt and Srath nan Aisinnin, (c) Stack of Glencoul – Gorm Loch Mor area of eastern Assynt, (d) upper reaches of Glen Cassley area of eastern Assynt, (e) southeastern Assynt including Allt nan Sleach stream section, indicating the complex structural relationships in the vicinity of the Moine thrust.

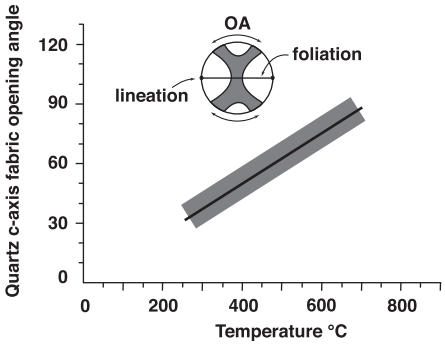

Fig. 4. Graph of quartz c-axis fabric opening angles vs. estimated deformation temperatures of naturally deformed quartz (Kruhl, 1998). Fabric opening angle (OA) illustrated in inset diagram. Gray bar indicates ±50 °C confidence limit for best-fit linear relationship between opening angle and temperature.

Moine nappe (Dallmeyer et al., 2001). If correct, these relationships constrain MTZ thrusting between 430 and 408 Ma, although it is possible that thrusting was complete by ~420 Ma.

4. Deformation temperatures and petrography

Temperatures of deformation discussed in this study were obtained using: (1) the quartz c-axis fabric opening-angle thermometer of Kruhl (1998), which has a graphically estimated error of ±50 °C (Fig. 4), and (2) the quartz recrystallization mechanism thermometer proposed by Stipp et al. (2002a,b), see examples of microstructures in Fig. 5, which provides a broader estimate of temperature as compared to the opening-angle thermometer. All estimated deformation temperatures are shown in Tables 1 and 2 and quartz c-axis fabrics used to estimate these temperatures are shown in Figs. 6–9.

4.1. Quartz c-axis opening-angle thermometer

During ductile deformation and dynamic recrystallization the opening angle of quartz c-axis fabrics increases with increasing deformation temperature, increasing hydrolytic weakening and/or decreasing strain rate, as indicated by experimental data (Tullis et al., 1973), numerical fabric simulation (Lister et al., 1978; Lister and Hobbs, 1980) and analysis of natural tectonites in which deformation temperatures are independently constrained (e.g. Lister and Dornsiepen, 1982; Morgan and Law, 2004). Kruhl (1998) has suggested that the opening angles of c-axis fabrics may be used as deformation thermometer (Fig. 4), assuming that deformation temperature is the prime factor controlling opening angle.

Taylor-Bishop-Hill (TBH) modeling of quartz c-axis fabric development suggests that fabric opening angle may also be sensitive to variation in 3-D strain. For example, simulations by Lister and Hobbs (1980) in which only dislocation glide is considered indicate that, for a given set of slip systems, opening angle decreases from flattening to plane strain to constrictional flow. For TBH modeling that produced Type 1 cross-girdle fabrics (Lister and Hobbs, 1980, their Fig. 8) similar to those measured in the Moine thrust zone mylonites, opening angle decreased from 56° ($k = 0$) to 51° ($k = 1$). This 5° difference in opening angle would correspond to a difference of approximately 30 °C using the Kruhl thermometer. For the Moine thrust zone mylonites reported in this study, quantitative 3-D strain data, indicating general flattening ($1 > k > 0$) strains, are only available for samples collected from the Stack of Glencoul (Law et al., 2007, 2010). However, almost all of our samples are foliated and variably lineated, and are also characterized by single or cross-girdle c-axis fabrics indicating plane strain – general flattening strains.

The presence or absence of dynamic recrystallization also has an influence on quartz c-axis fabric opening angle. Recrystallized grains in both experimentally and naturally deformed quartzites almost always yield larger c-axis fabric opening angles than those measured on adjacent detrital grains which deformed solely by dislocation creep (Tullis et al., 1973; Law, 1986; Law et al., 2010). The opening angles reported here for the MTZ mylonites were measured using fabrics obtained from both optical (universal stage) and electron backscatter diffraction (EBSD) techniques. The quartz c-axis fabric of one sample (F-8 of Strine and Mitra, 2004) reported here was obtained using x-ray texture goniometry (XRTG). Both dynamically recrystallized and original detrital grains are observed in the mylonitic Cambrian quartzites located beneath the Moine thrust (Law et al., 1984, 1986, 2010), whereas only recrystallized quartz grains are observed in the mylonitic Moine psammites of the overlying Moine nappe.

Our optical fabrics were with two exceptions (see below) exclusively measured on dynamically recrystallized grains. In contrast, our EBSD analyses were automated and did not allow for discrimination between detrital and recrystallized grain fabrics. However, thin section analysis of the Cambrian quartzites samples analyzed by EBSD generally indicates only minor preservation of detrital grains within a matrix of recrystallized grains. EBSD analyses were conducted at the Leeds Electron Microscopy and Spectroscopy (LEMAS) Centre, University of Leeds, using a Camscan Series 4 Scanning Electron Microscope (SEM) fitted with an HKL/Oxford Diffraction Channel 5 Imaging System. Operating conditions for the SEM-EBSD include a 20 kV accelerating voltage and ~20 nA specimen current. For indexing of EBSD patterns, we used the HKL quartz-new phase files with pattern fitting based on 6 diffraction bands and a mean angular deviation of 1. Beam step size was determined by sample mean grain size to index ~1 pattern per grain. Both optical and EBSD analyses were conducted on sections cut perpendicular to foliation and parallel to the ESE trending mineral lineation.

4.2. Quartz recrystallization mechanism thermometer

Stipp et al. (2002a,b) have suggested that quartz recrystallization regime may also be used as a deformation thermometer, assuming "average" geologic strain rates. The regimes include grain-boundary bulging (GBB), subgrain rotation (SGR) and grain-boundary migration (GBM). From an integrated analysis of experimentally and naturally deformed samples, they suggested that under natural conditions GBB is the dominant recrystallization mechanism at 270–390 °C, SGR is dominant at 410–490 °C, and GBM is dominant at >520 °C, with a transition from GBB to SGR at 390–410 °C, and from SGR to GBM at 490–520 °C.

4.3. Mylonitic thrust sheet beneath the ductile Moine thrust – petrography

The mylonitic thrust sheet(s) beneath the Moine thrust contain two lithotectonic units, the Archaean Lewisian basement gneiss and the Cambrian Eriboll Formation. Mylonitic Lewisian units contain quartz, plagioclase, K-feldspar, muscovite, and chlorite with accessory ilmenite, magnetite, zircon, apatite, and allanite. Elongate recrystallized quartz grains and laths of muscovite and chlorite define the mesoscopic foliation. Shear bands, indicating both top-to-the-west and top-to-the-east shear senses, are commonly localized along phyllosilicate-rich horizons. Top-to-the-west shear bands are dominant and more pervasive. Recrystallized tails surrounding rotated porphyroclasts all indicate a top-to-the-west-northwest shear sense (Fig. 5a).

The overlying mylonitic Cambrian Eriboll Formation is dominantly composed of quartzite with lesser amounts of quartzo-feldspathic psammite and quartz-muscovite schist. Foliation is

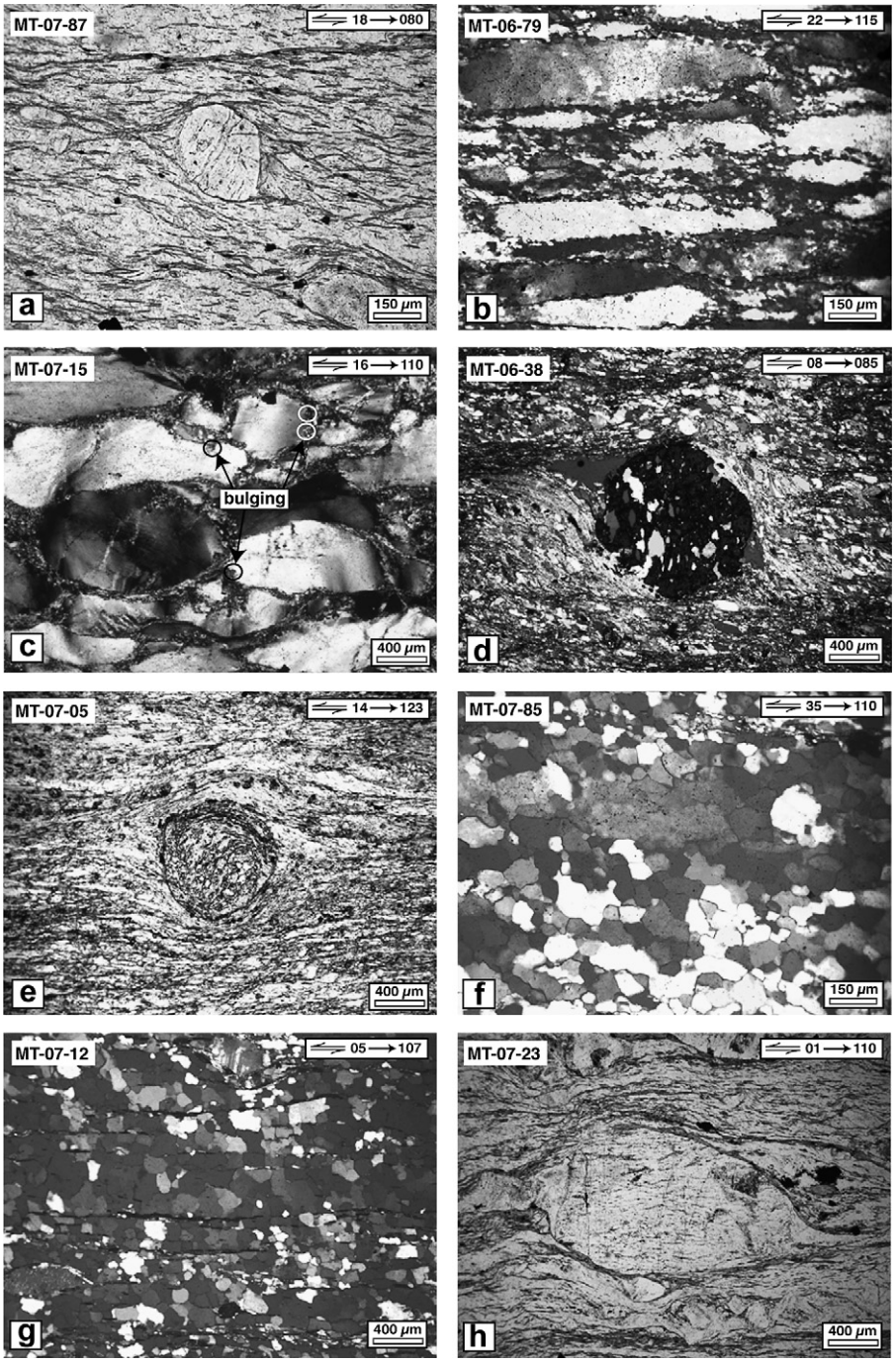

Fig. 5. Photomicrographs of samples from the study area. All sections are parallel to mineral lineation, perpendicular to foliation, and viewed toward the NNE. Sample grid coordinates shown in Table 3. Profile direction and shear sense shown in upper righthand corner of each photomicrograph. (a) Lewisian gneiss with rigid feldspar porphyroclasts in quartz and phyllosilicate matrix. Tails indicate top-to-the-west-northwest shear sense. (b) Core and mantle structure and oblique grain shape fabric in mylonitic Cambrian quartzite. (c) Microstructures indicating grain-boundary bulging recrystallization in mylonitic Cambrian quartzite from southern Assynt (sample MT-07-15; location shown in Fig. 2a). (d) Moine quartz-muscovite schist with euhedral to subhedral garnet containing curved inclusion trails that are discordant to the mesoscopic foliation. Asymmetric tails indicate top-to-the-west-northwest shear sense. (e) Suhedral garnet with curved discordant inclusion trails wrapped by foliation, which is defined by elongate quartz grains and muscovite-bioitite laths. (f and g) Quartz grains with seriate, irregular grain boundaries in Moine psammite indicating relatively unpinned grain-boundary migration recrystallization of quartz; in (g) quartz grain size is controlled to some degree by pinning of grain boundaries by thin phyllosilicate layers, which defines the foliation. (h) Feldspar porphyroclast wrapped by muscovite and biotite folation in Moine psammite. Tails indicate top-to-the-west-northwest sense of shear.

defined by elongate recrystallized quartz grains and phyllosilicate laths. However, in less intensely strained and dynamically recrystallized quartzites located near the contact between the mylonitic thrust sheets and the lower MTZ in the Loch More – Stack of Glencoul region, elongate relict quartz grains are aligned parallel to the mesoscopic foliation.

4.4. Mylonitic thrust sheet beneath the ductile Moine thrust – deformation temperatures

In the mylonitic thrust sheets beneath the Moine thrust, quartz recrystallization dominantly occurs by SGR with GBB recognized only at the structurally lowest levels. Adopting the Stipp et al.

Table 1
Quartz c-axis opening angles and corresponding deformation temperature estimates for samples in the footwall to the Moine thrust.

Sample	Opening angle (°)	Deformation T (°C)	[a]Method	[b]Qtz recryst.	[c]Grain type	[d]BNGRS coordinates
MT-06-79	48	385	EBSD	GBB-SGR	n/a	NC 31847 37541
[e]F-8	53	425	[h]XRTG	Unknown	n/a	Unavailable
[e]F-7	55	440	Optical	Unknown	n/a	Unavailable
[e]F-6	49	395	Optical	Unknown	n/a	Unavailable
[e]F-5	56	450	Optical	Unknown	n/a	Unavailable
[e]F-4	51	410	Optical	Unknown	n/a	Unavailable
MT-03-01	58	450	Optical	SGR	Detrital	NC 31500 32450
MT-07-71	47	380	EBSD	GBB-SGR	n/a	NC 31539 32408
MT-07-71	54	425	Optical	GBB-SGR	Detrital	NC 31539 32408
MT-07-105	48	385	EBSD	GBB-SGR	n/a	NC 28950 29800
[f]SG-13	63	505	Optical	SGR	Recrystallized	NC 28930 28680
[f]SG-11	63	505	Optical	SGR	Recrystallized	NC 28930 28680
[f]SG-10	68	545	Optical	SGR	Recrystallized	NC 28880 28760
[f]SG-9	68	545	Optical	SGR	Recrystallized	NC 28930 28680
[f]SG-8	67	535	Optical	SGR	Recrystallized	NC 28930 28680
[f]SG-7	68	545	Optical	SGR	Recrystallized	NC 28930 28681
[f]SG-6	68	545	Optical	SGR	Recrystallized	NC 28930 28682
[f]SG-4	63	505	Optical	SGR	Recrystallized	NC 28880 28760
[f]SG-3	54	435	Optical	SGR	Recrystallized	NC 28880 28761
[f]SG-2.5	62	500	Optical	SGR	Recrystallized	NC 28880 28762
[f]SG-2.4	60	480	Optical	SGR	Recrystallized	NC 28880 28763
[f]SG-2.3	62	500	Optical	SGR	Recrystallized	NC 28880 28764
[f]SG-2.2	68	545	Optical	SGR	Recrystallized	NC 28880 28765
[f]SG-2.1	63	505	Optical	SGR	Recrystallized	NC 28880 28766
[f]SG-1	55	445	Optical	SGR	Recrystallized	NC 28880 28700
[g]GM-2	59	470	Optical	SGR-GBM	Recrystallized	NC 30500 26400
[g]GM-1	64	510	Optical	SGR-GBM	Recrystallized	NC 30700 26500
MT-07-88	72	575	Optical	GBM	Recrystallized	NC 30950 26300
[g]GM-3	62	500	Optical	SGR-GBM	Recrystallized	NC 32550 24900
MT-07-76	71	560	Optical	GBM	Recrystallized	NC 34244 23121
MT-07-21	74	580	Optical	GBM	Recrystallized	NC 34900 17399
[g]AS-2	62	500	Optical	GBM	Recrystallized	NC 32100 09400
[g]AS-3	62	500	Optical	GBM	Recrystallized	NC 32100 09401
[g]AS-4	69	550	Optical	GBM	Recrystallized	NC 32100 09402
[g]AS-7	59	470	Optical	GBM	Recrystallized	NC 32100 09404
[g]AS-8	61	490	Optical	GBM	Recrystallized	NC 32100 09405
[g]AS-9	62	500	Optical	GBM	Recrystallized	NC 32100 09406
[g]AS-10	62	500	Optical	GBM	Recrystallized	NC 32100 09407
[g]AS-11	67	535	Optical	GBM	Recrystallized	NC 32100 09408
[g]AS-12	66	530	Optical	GBM	Recrystallized	NC 32100 09409
[g]82-111	58	465	Optical	GBM	Recrystallized	NC 32100 09410
MT-07-20	59	470	EBSD	SGR	n/a	NC 29100 06400

[a] Quartz c-axis fabrics obtained using either optical (universal stage microscope) or automated (EBSD) methods.
[b] Quartz recrystallization mechanism; GBB-Grain-boundary bulging, SGR-Subgrain rotation, GBM-Grain-boundary migration.
[c] Type of grains measured (detrital vs. recrystallized) for optical analyses; not applicable for EBSD analyses.
[d] British National Grid Reference System.
[e] Samples of Strine and Mitra (2004) and Strine and Wojtal (2004).
[f] Samples of Law et al. (in press).
[g] Samples of Law et al. (1986).
[h] X-ray texture goniometry.

Table 2
Quartz c-axis opening angles and corresponding deformation temperature estimates for samples in the hangingwall to the Moine thrust.

Sample No	Opening angle (°)	Deformation T (°C)	[a]Method	[b]Qtz recryst.	[c]Grain type	[d]BNGRS coordinates
[e]M-1	51	405	Optical	SGR	Recrystallized	NC 28880 28760
[e]M-3	57	450	Optical	SGR	Recrystallized	NC 28930 28680
[f]GM-4	73	585	Optical	GBM	Recrystallized	NC 32600 25100
MT-07-78	72	575	Optical	GBM	Recrystallized	NC 33563 24353
MT-07-75	72	575	Optical	GBM	Recrystallized	NC 34480 23148
MT-07-80	75	590	Optical	GBM	Recrystallized	NC 35502 21043
MT-07-22	74	580	Optical	GBM	Recrystallized	NC 35049 17449
[f]AS-1	70	560	Optical	GBM	Recrystallized	NC 32150 09500
[f]AS-6	65	520	Optical	GBM	Recrystallized	NC 32150 09500

[a] Quartz c-axis fabrics obtained using either optical (universal stage microscope) or automated (EBSD) methods.
[b] Quartz recrystallization mechanism; GBB-Grain-boundary bulging, SGR-Subgrain rotation, GBM-Grain-boundary migration.
[c] Type of grains measured (detrital vs. recrystallized) for optical analyses; not applicable for EBSD analyses.
[d] British National Grid Reference System.
[e] Samples of Law et al. (in press).
[f] Samples of Law et al. (1986).

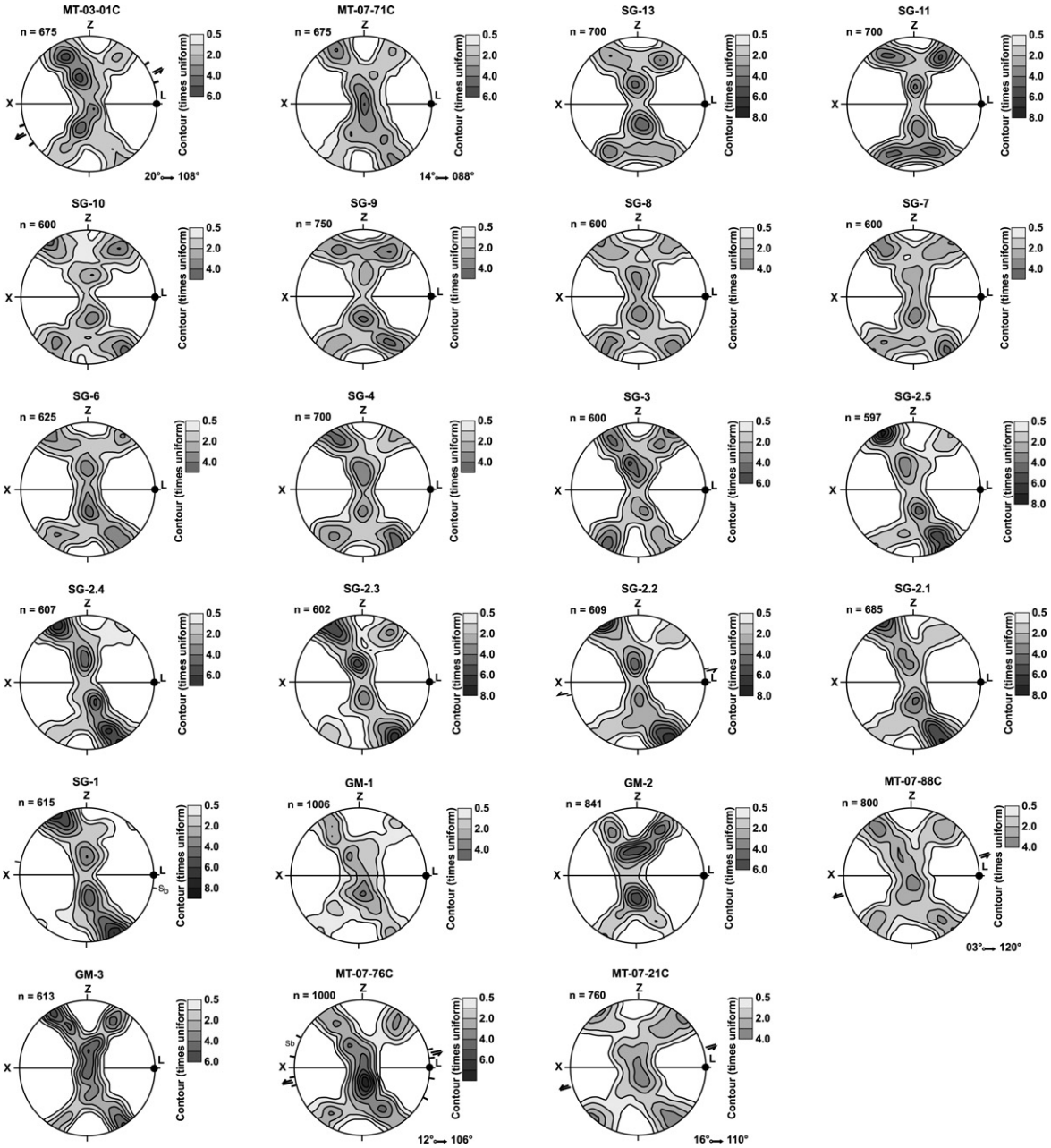

Fig. 6. Quartz c-axis fabrics obtained using optical techniques for mylonitic Cambrian quartzites in footwall to the ductile Moine thrust. All fabric diagrams are lower hemisphere, equal-area projections shown looking NNE; foliation oriented left to right, lineation horizontal. Samples are from this study (prefix MT), Law et al. in press (prefix SG), and Law et al., 1986 (prefix GM).

(2002a,b) thermometer, this contrast in dominant recrystallization mechanism indicates deformation temperatures of <400 °C (GBB) and 400–500 °C (SGR) for the lower and higher levels of the thrust sheet, respectively. Additionally, along strike variation in recrystallization mechanisms are also recognized. For example, while recrystallization by SGR is dominant at the Stack of Glencoul, from the Stack southward to the Loch Ailsh intrusive complex (Fig. 2), recrystallization by GBM is pervasive and suggests higher (>520 °C) deformation temperatures.

Deformation temperatures estimated from quartz c-axis fabric opening angle (Table 1) yield similar results to temperatures obtained using the Stipp et al. (2002a,b) thermometer. From Loch More to just north of the Stack of Glencoul, estimated deformation temperatures range from 380 to 450 °C. Sample MT-06-79, collected immediately south of Loch More, yields a constrictional quartz a-axis fabric, which may indicate that the deformation temperature of 385 °C may be an underestimate. South of Srath nan Aisinnin, sample MT-07-71 yields contrasting deformation temperature estimates for EBSD (380 °C) and optically (425 °C) measured c-axis fabrics, respectively. We believe these differences are simply an artifact of the inability of EBSD techniques to discriminate between detrital and recrystallized grains, and hence fabrics obtained using EBSD represent bimodal grain type distributions. Quartz recrystallization in all of these samples is by SGR with no microstructural evidence for significant GBM.

At the Stack of Glencoul, Law et al. (1986) and Law (1987) reported crystal fabrics of a suite of 13 mylonitic Cambrian quartzite samples (SG series in Table 1 and Fig. 6) in the Moine thrust footwall. Fabrics measured on detrital grains yield deformation temperatures of 380–450 °C, while fabrics measured on

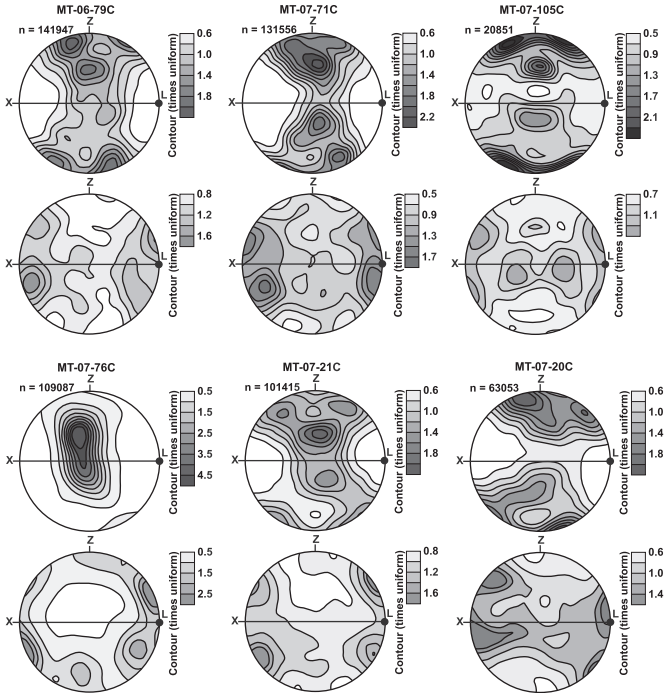

Fig. 7. Quartz c- and a-axis axis fabrics obtained using electron backscatter diffraction (EBSD) techniques for mylonitic Cambrian quartzites in footwall to the ductile Moine thrust. For each sample: c-axis fabric – upper diagram; a-axis fabric – lower diagram. All fabric diagrams are lower hemisphere, equal-area projections shown looking NNE; foliation oriented left to right, lineation horizontal.

matrix recrystallized grains indicate deformation temperatures of 435–545 °C (Law et al., 2010). Recrystallization in these mylonites is by SGR, suggesting deformation temperatures of 410–490 °C (Stipp et al., 2002a,b). Law et al. (2010) believe these inferred deformation temperatures to be too high and have speculated that the recrystallized grain fabrics may result from greater hydrolytic weakening in the fine-grained matrix grains, with fine-grained white mica formed along grain boundaries inhibiting GBM. Additionally, the general flattening strains (K values of 0.37–0.58; Law et al., 2010) in the mylonites may cause some overestimation of deformation temperature.

Further south in the Gorm Loch Mor region, mylonitic Cambrian quartzite samples yield deformation temperatures of 470–575 °C based on quartz c-axis fabrics of recrystallized grains (Table 1; Fig. 6). Recrystallized quartz grains in these samples are larger than in the Stack mylonites (25–40 microns as compared to <15 microns) and recrystallization is dominantly by GBM with limited evidence for SGR. In eastern Assynt, samples MT-07-76 and MT-07-21 yield deformation temperatures of 560 °C and 580 °C, respectively. Recrystallization occurs exclusively by GBM, indicating deformation temperatures of >520 °C (Stipp et al., 2002a,b). In sample MT-07-21, which is located 2 km north of the Loch Ailsh intrusive complex, trails of minute foliation-parallel micas within the large (150–400 micron) equant quartz grains indicate high grain boundary mobility, and hence relatively high deformation temperatures. In the Allt nan Sleach stream section in southeastern Assynt, optically measured quartz c-axis fabrics reported by Law et al. (1986) from recrystallized Cambrian quartzites indicate deformation temperatures of 465–550 °C. Recrystallization is dominated by GBM in the mono-mineralic quartzites and grain size varies from 40 to 60 microns. Grain boundary pinning and smaller grain sizes (with limited microstructural evidence for SGR) are observed, however, in the more micaceous quartzites. These apparently relatively high temperature Allt nan Sleach quartz mylonites are located within 1 km of the Loch Ailsh alkaline intrusive complex and are directly associated with intrusion of at least one synkinematic alkaline (nordmarkite) sill (Law et al., 1986). Further south and a greater distance from the Loch Ailsh intrusion, sample MT-07-20 yields a deformation temperature of 470 °C and quartz recrystallization occurs exclusively by SGR.

4.5. Moine nappe – petrography

Rocks of the Moine nappe generally consist of feldspathic-micaceous psammite and quartzite, with lesser pelite and semipelite and rare amphibolite (Holdsworth et al., 2001). Moine psammite samples are dominantly composed of a quartz and phyllosilicate matrix with a variable abundance of feldspar, epidote, and opaque porphyroclasts. At relatively low structural levels (<200 m above the Moine thrust), phyllosilicate layers are dominated by muscovite and chlorite, but biotite becomes increasingly abundant toward the east and south. Garnet grains, where present, are subhedral to euhedral, and north of Assynt are observed to contain up to two distinct growth zones (Thigpen, 2009, see also early descriptions by Read, 1931, pp. 46–50 and Bailey, 1955, p. 117). Some garnet cores contain curved inclusion trails that are discordant to the dominant enveloping foliation (Fig. 5d and e), which is defined by elongate quartz grains and phyllosilicate laths. Dynamic

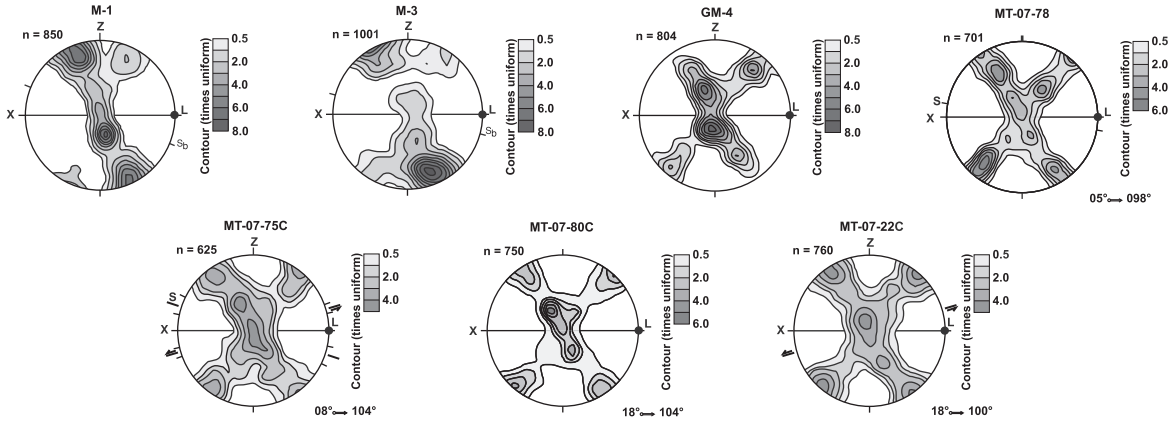

Fig. 8. Quartz c-axis fabrics obtained using optical techniques for Moine mylonites in the hangingwall to the Moine thrust. All fabric diagrams are lower hemisphere, equal-area projections shown looking NNE; foliation oriented left to right, lineation horizontal. Samples are from this study (prefix MT), Law et al. in press (prefix M), and Law et al., 1986 (prefix GM). Note: fabrics M-1 and M-2 are from dynamically recrystallized foliation-parallel quartz veins. All other fabrics are from dynamically recrystallized grains dispersed within matrix of deformed metasedimentary rocks.

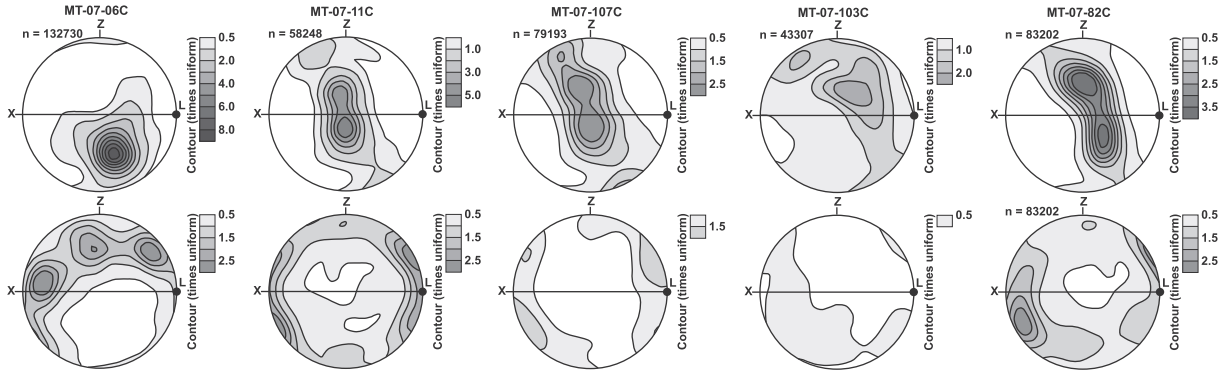

Fig. 9. Quartz c-axis fabrics obtained using electron backscatter diffraction (EBSD) for Moine mylonites in hangingwall to the Moine thrust. Upper row: c-axis fabrics; lower row – a-axis fabrics. All fabric diagrams are lower hemisphere, equal-area projections shown looking NNE; foliation oriented left to right, lineation horizontal.

recrystallization of quartz in our Moine samples is dominantly by GBM, as indicated by mostly strain free grains with deeply sutured grain boundaries (Fig. 5f). In quartz-rich samples exhibiting GBM, grain size is controlled to some degree by the variable abundance and spacing of phyllosilicate laths, which act to "pin" the mobile quartz grain boundaries (Fig. 5g). Tails of rotated porphyroclasts (Fig. 5h), oblique grain shape fabrics, and mica fish all indicate a top-to-the-west-northwest sense of shear.

4.6. Moine nappe – deformation temperatures

Between Loch More and the Stack of Glencoul, rocks in the hangingwall to the Moine thrust are dominantly pelitic and hence are rarely suitable for quartz petrofabric analysis. Additionally, quartz c-axis analyses of five mylonitic Moine samples from this area have yielded point maxima or single-girdle c-axis fabrics (Fig. 9), which cannot be used for thermometry. Two samples (M-1 and M-3 of Law et al., 2007, 2010) of dynamically recrystallized foliation-parallel quartz veins with optically measured cross-girdle fabrics in Moine mylonites at the Stack of Glencoul (Fig. 8) yield deformation temperatures of 405–450 °C. However, it is unclear if these fabrics are representative of deformation conditions in the surrounding, dominantly pelitic, mylonitic Moine rocks.

South of the Stack of Glencoul, quartz content in the Moine mylonites increases sufficiently for meaningful petrofabric analysis. Strongly defined transitional Type 1–Type 2 cross-girdle c-axis fabrics (Lister, 1977) were measured optically and yield deformation temperatures of 575–590 °C (Table 2). Quartz recrystallization is by GBM in all these mylonites, indicating deformation temperatures of >520 °C (Stipp et al., 2002a,b). In southern Assynt, quartz c-axis fabrics reported by Law et al. (1986) from mylonitic Moine samples of the Allt nan Sleach stream section yield deformation temperatures of 520–560 °C (Table 2), although the fabric in sample AS-1 is dominated by an asymmetric single girdle and the opening angle and estimated deformation temperature are therefore poorly defined.

4.7. Structural interpretation of deformation temperature distribution

In the Gorm Loch Mor area (Fig. 2), higher deformation temperatures are indicated by the opening-angle thermometer in the Moine mylonites (sample GM-4; 585 °C) than in the adjacent footwall (sample GM-3; 500 °C). Although less clearly defined, a similar difference in deformation temperatures is also indicated by cross-girdle fabrics in hangingwall Moine mylonites (520–560 °C) and adjacent footwall quartzites (465–530 °C) in the Allt nan Sleach stream section of southern Assynt (Fig. 2). This suggests that at least locally the ductile Moine thrust, which emplaces mylonitic Moines over similarly deformed Cambrian quartzite, is a thermal ramp.

Between the Gorm Loch Mor and Allt nan Sleach localities, however, almost identical deformation temperatures are indicated by optically measured c-axis fabric opening angles in adjacent mylonitic Moine samples and Cambrian quartzite (575 vs 560 °C in samples MT-07-76 and 75; 580 °C in both samples MT-07-21 and 22). This suggests that at least locally the ductile Moine thrust is either a thermal flat or that dynamic recrystallization and associated fabric development post-dates motion on the ductile Moine thrust. Microstructural and crystal fabric evidence at the Stack of Glencoul (Law et al., 1986, 2010; Knipe, 1990) strongly indicates that motion on the ductile Moine thrust occurred either synchronously with, or outlasted, dynamic recrystallization and crystal fabric development in both the hangingwall and footwall rocks. This supports the former interpretation of the ductile Moine thrust locally being a thermal flat.

Within the Assynt region, the highest deformation temperatures in the Moine thrust footwall are recorded to the east and north of the Loch Ailsh intrusive complex (Fig. 2). This could indicate that higher temperature (more hinterland) quartzites were accreted on to the footwall to the ductile Moine thrust in this area, while cooler (more foreland) quartzites were accreted on to the footwall in the Stack of Glencoul area to the north. Alternatively, our thermal data could indicate that at least the waning stages of mylonitization on the ductile Moine thrust occurred during cooling of the Loch Ailsh Complex with heat transfer from the intrusion to the adjacent belt of developing mylonites (Law and Johnson, 2010). However, the highest estimated deformation temperature, supported by microstructural evidence for high grain boundary mobility, in our suite of Cambrian quartzite samples is actually recorded in sample MT-07-21 (see above) located ~2 km north of the ultramafic members of the Loch Ailsh intrusive suite, possibly indicating an underlying subsurface extension of the intrusion.

Intuitively, these inferred deformation temperatures seem too high for mylonites that are traditionally thought to have developed under lower greenschist facies conditions (Johnson et al., 1985). The local presence of euhedral garnet in the Moine mylonites at the leading edge of the Moine nappe (Thigpen, 2009) may indicate that deformation may have originally occurred under garnet grade conditions, as originally suggested by MacGregor (1952) at the southern end of the MTZ (see review by Law and Johnson, 2010). However, the age of garnet growth (Scandian or older) at the leading edge of the Moine nappe remains to be established. Similarly the local presence/preservation of biotite in the mylonites at the leading edge of the Moine nappe (Thigpen, 2009; see also descriptions and discussion by Read, 1931, pp. 46–50; Bailey, 1955, pp. 114–117) suggests at least upper greenschist facies (>c. 450 °C)

conditions during early mylonitization. For example, foliation-parallel red biotite grains forming asymmetric wings on small garnet grains (top to WNW shear sense) are recorded from a sample lying immediately above the Moine thrust plane in the Strath nan Aisinnin area of northern Assynt (Fig. 2).

Certainly an excellent correlation is noted in all samples between deformation temperature ranges indicated by quartz recrystallization regime (Stipp et al., 2002a,b) and specific temperatures indicated by quartz c-axis fabric opening angle (Kruhl, 1998). However, as both recrystallization regime and fabric opening angle are potentially sensitive to hydrolytic weakening and strain rate, the possibility must remain that our data could also reflect spatial variations in these environmental variables. Clearly what is needed here is an independent measure of deformation temperature that is insensitive to these variables. The titanium in quartz thermometer (see review by Kohn and Northrup, 2009) may be a potential research tool for future work on discriminating between these possibilities.

5. 3-D strain – analytical methods and results

Strain markers are rarely preserved in the quartz-rich mylonites of this study due to total dynamic recrystallization. Some important exceptions exist to this general rule in the mylonitic Cambrian quartzites located beneath the Moine thrust plane in northern Assynt. For example, deformed detrital grains are at least partially preserved in mylonitic Cambrian quartzites exposed at the Stack of Glencoul (Fig. 2) and have been used as 3-D strain markers (Law et al., 2007, 2010). General flattening strains (Flinn's K parameter ranging between 0.37 and 0.58) are recorded in all of these samples. Similarly, general flattening strains ($K = 0.2–0.4$) are indicated in mylonitic, partially recrystallized Cambrian quartzites (e.g. samples MT-03-01 and 07-71; Table 1, Fig. 2) exposed in a vertical stream transect in the Strath nan Aisinnin area of northernmost Assynt (B. Roth personal communication, 2009). Strine and Mitra (2004) identified both relict detrital and recrystallized grains in at least some mylonitic Cambrian quartzites in the Strath nan Aisinnin and Stack of Glencoul areas with oblate fabrics, although the validity of using recrystallized grains as strain markers remains uncertain.

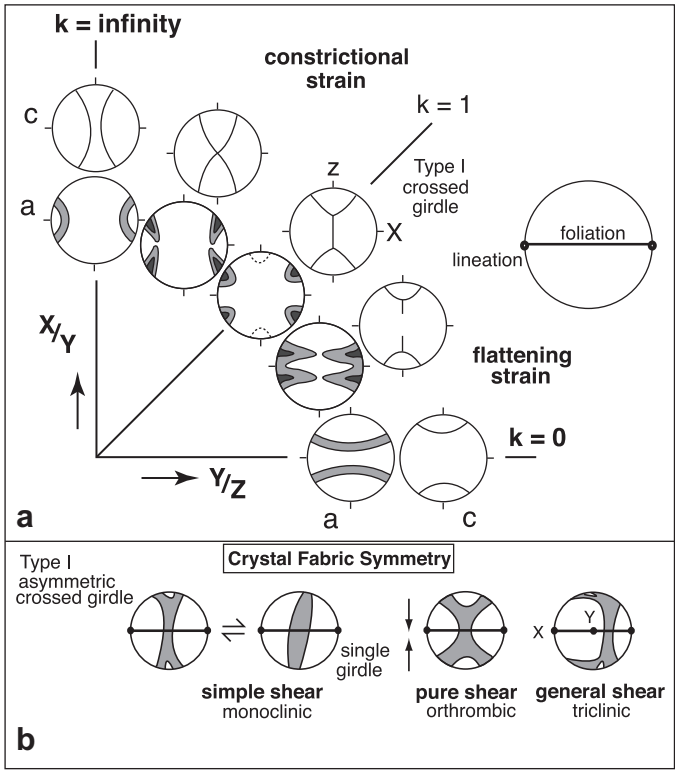

Fig. 10. (a) Relationships between strain symmetry and quartz c-axis and a-axis fabrics for coaxial deformation; c-axis fabrics represented by fabric skeletons; modified from Schmid and Casey (1986). (b) Relationships between deformation path (e.g. simple shear vs. pure shear) and c-axis fabrics. For simple shear, the c-axes form either an asymmetric crossed girdle or a single girdle; asymmetry of c-axis fabrics to foliation and lineation is used to infer shear sense, dextral in this example. For pure shear (coaxial deformation), c-axis fabrics are symmetric with respect to foliation and lineation. For triclinic shear, grain-shape lineation may be oblique to kinematic framework.

Given the overall rarity of strain markers, we infer 3-D strain type from the pattern of quartz c- and a-axis fabrics measured by optical methods, EBSD analysis (this study), or X-ray texture goniometry (Law et al., 1986) in these mylonites. For at least coaxial deformation histories, quartz c- and a-axis fabric patterns in both natural deformation and in experimental and numerical modeling studies appear to vary smoothly with 3-D strain (see reviews by Price, 1985; Schmid and Casey, 1986; Law, 1990), leading to the possibility that the pattern of quartz c-axis fabric, and particularly the a-axis fabric, can be used as a qualitative indicator of 3-D strain (flattening, plane strain, constriction). Predicted relationships between 3-D strain and pattern of quartz c- and a-axis fabrics are summarized in Fig. 10.

5.1. Quartz c- and a-axis fabrics – 3-D strain interpretation

Fabrics from the majority of our samples indicate general flattening ($1 > K > 0$) to approximate plane strain ($K \sim 1$) conditions. Fabrics indicative of general flattening strains are particularly common in the mylonitic Cambrian quartzites. In northern Assynt, samples MT-03-01 and MT-07-71 are characterized by Type 1 (Lister, 1977) cross-girdle c-axis fabrics and a-axis fabrics, which contain both a-axis point maxima oriented in the XZ plane and a partial girdle centered about the foliation pole (Figs. 6 and 7). Similar, although more clearly defined fabrics, have been recorded in mylonitic Cambrian quartzites at the Stack of Glencoul (Fig. 6, Law et al., 1986, 2010) where 3-D strain analysis of relict detrital grains shapes also indicates general flattening strains (Law et al., 2007, 2010). A small circle girdle of c-axes centered about the foliation pole is variably developed in the Type 1 cross-girdle fabrics exhibited by the mylonitic Cambrian quartzites at the Stack, but in general the a-axis fabrics seem to better reflect the general flattening deformation indicated by 3-D strain analysis. These general flattening to approximately plane strain fabrics continue southwards along strike in the mylonitic Cambrian quartzites toward the Loch Ailsh intrusive complex, with well defined small circle a-axis fabrics indicative of general flattening being recorded in samples MT-07-21 and MT-07-20 (Fig. 7).

Fabrics indicative of plane strain ($K \sim 1$) to general constriction ($\infty > K > 1$) in the mylonitic Cambrian quartzites have only been recorded immediately to the south of Loch More and in the Allt nan Sleach stream section (Fig. 2). Sample MT-06-79, collected on the south side of Loch More, yields a c-axis fabric that is transitional between a cross-girdle fabric and a small circle fabric of large opening angle centered about the lineation (Fig. 8), suggesting deformation transitional between plane strain and constriction (Fig. 10a). This is confirmed by the a-axis fabric that, in addition to point maxima in the XZ plane, also contains a small circle girdle of moderate opening angle centered about the lineation (Fig. 8). Similarly, the Allt nan Sleach mylonites are characterized by transitional Type 1–2 (Lister, 1977) cross-girdle c-axis and a-axis fabrics that in addition to point maxima in the XZ plane also contain partial small circle girdles centered about the lineation, indicating slightly constrictional strains (Law et al., 1986). Interestingly, both the Loch

More and Allt nan Sleach sample sites are located on WNW trending thrust transport-parallel lineaments that can be traced eastwards into the Moine nappe. While the lineament passing through Loch More has, to date, only been recognized as a prominent topographic feature, the lineament passing close to the Allt nan Sleach section marks the approximate position of the Oykel Transverse Zone (Leslie et al., 2010). This is a steeply dipping, 5 km wide and c. 20 km long shear zone in the overlying Moine nappe that is characterized by constrictional fabrics aligned parallel to the regional WNW directed thrust transport direction.

In the Moine mylonites, strongly developed transitional Type 1–2 (Lister, 1977) cross-girdle c-axis fabrics are recorded by optical analysis, while broad single girdle to point maxima fabrics are obtained by EBSD analysis (Figs. 8 and 9). This difference between optical and EBSD generated fabrics is likely associated with contouring statistics of the EBSD data and the difficulty of recording grains on the less strongly populated trailing edge of the fabric skeleton. Both the cross-girdle and single-girdle fabrics indicate approximate plane strain deformation (cf. Fig. 10), although the tendency toward Type 2 cross-girdles could indicate either higher deformation temperatures and/or lower strain rates than associated with Type 1 cross-girdle fabrics (as dominantly recorded in the underlying Cambrian quartzites) or slightly constrictional strains (see discussion by Schmid and Casey, 1986, pp. 281–282).

5.2. Quartz c- and a-axis fabrics – qualitative kinematic interpretation

Asymmetry in our measured cross-girdle c-axis fabrics and the associated a-axis fabrics from both the mylonitic Cambrian quartzites and the overlying Moines is generally subtle, both in terms of skeletal outline and density distribution (Figs. 6–9). Asymmetries are consistent with a top to the WNW shear sense, but at least qualitatively would suggest a significant component of coaxial (pure shear) deformation. Transitional cross-girdle to single girdle quartz c-axis fabrics and their associated a-axis fabrics adjacent to the ductile Moine thrust are known to be strongly asymmetric (Fig. 6, samples SG-1–SG-2.5), and the sense of asymmetry also indicates a top to the WNW shear sense (Law et al., 1986, 2010; Law, 1987, 2010). Single-girdle fabrics obtained by EBSD analysis in Cambrian quartzites (Fig. 8, sample MT-07-76) and Moine rocks (Fig. 9) are also compatible with a top to the WNW shear sense.

6. Rigid grain vorticity analyses: methods

Numerous techniques for quantitative analysis of flow vorticity in naturally deformed rocks have been proposed (see review by Passchier and Trouw, 2005). However, the contrasting mechanical behavior of the different mineral phases in our MTZ mylonite samples (mostly rigid feldspar, epidote, and opaques in a ductile quartz and phyllosilicate matrix) make them ideal for rigid grain techniques (Passchier, 1987; Wallis et al., 1993; Jessup et al., 2007). In ductile, non-coaxial flow, rigid objects rotating in a flowing ductile matrix should, as a function of their axial ratio, either rotate infinitely or reach stable sink positions at high finite strain (Passchier, 1987). The stable sink position reached by rigid grains with large axial shape ratios is in turn a function of their orientation with respect to the eigenvectors of flow and the instantaneous stretching axes. The angle between these eigenvectors is numerically related to the mean kinematic vorticity number (W_m), where W_m equals the cosine of the acute angle between the flow apophyses.

The magnitude of W_m is a non-linear quantity varying between 0 (100% pure shear) and 1 (100% simple shear), with equal contribution of both simple and pure shear occurring at a W_m value of ~0.71 (Law et al., 2004). The rigid grain orientation method of Wallis et al. (1993) involves measurement of both the axial ratio of each rigid grain and the angle between the clast long axis and the macroscopic foliation (Figs. A1–A8) that is assumed to be oriented sub-parallel to one of the flow apophyses. Ideally, when clast axial ratio is plotted against the angle between clast long axis and mesoscopic foliation, a break should be recognized between grains of lower axial ratio that rotate infinitely having random orientations and those of higher axial ratio that reach stable sink positions sub-parallel to foliation. This break, known as the critical axial ratio (R_c), is mathematically related to the kinematic vorticity number (W_m) by the equation:

$$W_m = \left(R_c^2 - 1\right) \Big/ \left(R_c^2 + 1\right)$$

Observed angular relationships between macroscopic fabric elements (foliation and lineation) and quartz c- and a-axis crystal fabrics in our samples demonstrate, by analogy with experimental and numerical studies (see review by Law, 1990) that the mineral lineation in our samples developed parallel to the thrust transport direction and the maximum principal extension. Assuming monoclinic (but not triclinic) flow, this geometry means that thin sections cut perpendicular to foliation and parallel to lineation should be oriented orthogonal to the rotation axis of rigid grains. Because our data for the rigid grain method were collected on the inferred XZ plane of finite strain, they are not strictly valid for non-plane deformations, such as those indicated by quartz c- and particularly a-axis axis fabrics of samples from the Moine thrust mylonites. However, numerical analysis of non-plane strain situations by Tikoff and Fossen (1995) indicates that stretching parallel to the Y principal strain axis is likely to have only a very small effect (<0.05) on W_m estimates. The average error range for our vorticity estimates is ~0.07, which is due to the inherent ambiguity of determining R_c using the rigid grain method and is also greater than the error from this effect.

7. Rigid grain vorticity analyses: results

7.1. Southern Eriboll to Loch More

Between southern Eriboll and Loch More, 47 samples collected from the footwall and hangingwall to the Moine thrust (Fig. 2a, Tables 3 and 4) were found to be appropriate for rigid grain vorticity analysis techniques. Vorticity analyses of 21 mylonitic Lewisian basement gneiss samples in the footwall to the Moine thrust yield W_m estimates ranging from 0.52 to 0.83 (64–37% pure shear), with arithmetic mean minimum ($W_m$min) and arithmetic mean maximum ($W_m$max) vorticity values of 0.66 (53% pure shear) and 0.73 (47% pure shear), respectively. W_m estimates obtained from 25 mylonitic Moine psammite samples collected in the hangingwall of the ductile Moine thrust range from 0.55 (62% pure shear) to 0.78 (43% pure shear), with $W_m$min and $W_m$max voriticity values of 0.65 (55% pure shear) and 0.71 (50% pure shear), respectively. Sample MT-06-45, which is interpreted to lie within a structurally isolated thrust slice beneath the mylonitic thrust sheets that we tentatively correlate with the UA-CNF thrust sheet, yields a W_m estimate of 0.76–0.83 (45–37% pure shear).

7.2. Srath nan Aisinnin and Assynt

South of Loch More, 21 samples were selected for vorticity analysis from the Moine nappe and underlying mylonitic thrust sheets from Strath nan Aisinnin to immediately south of Knockan Crag (Fig. 2a; Tables 3 and 4). The lesser sampling density here is

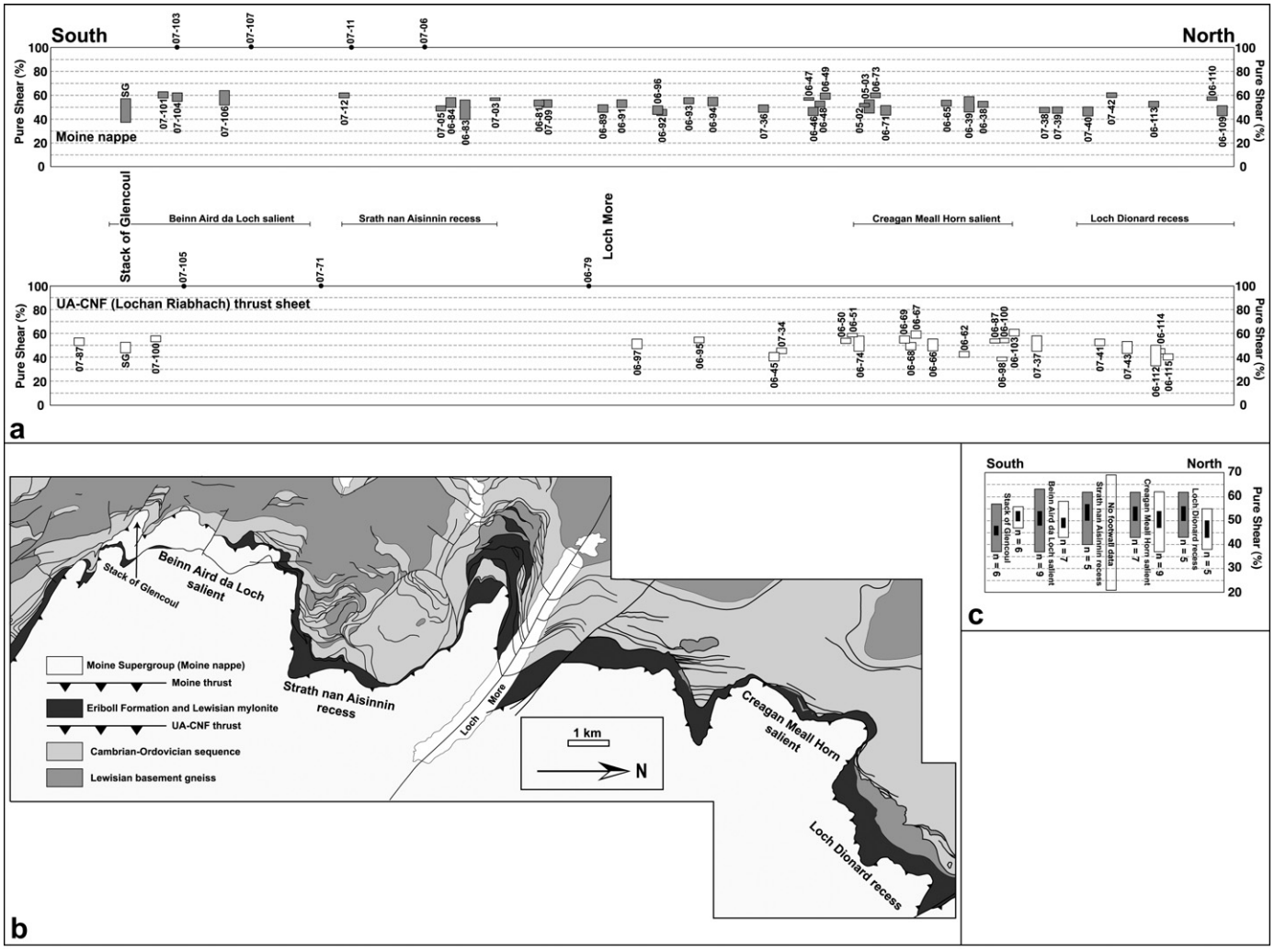

Fig. 11. (a) Along strike vorticity (W_m) profile from Loch Dionard to south of the Stack of Glencoul for the Moine nappe and mylonitic thrust sheet(s) in the footwall to Moine thrust that may be lateral equivalent(s) of the UA-CNF thrust sheet recognized at Loch Eriboll. Locations of the major salients, recesses, Loch More, and the Stack of Glencoul are shown. Locations of strain symmetry samples discussed in text are indicated at the top of each diagram. (b) Geologic map of profile area showing positions of major features. (c) Range of vorticity values (gray bars for hangingwall and white bars for footwall samples, respectively) and arithmetic mean minimum ($W_m$min) and mean maximum ($W_m$max) vorticity values (black bars) for samples collected in the Loch Dionard and Strath nan Aisinnin recesses, the Creagan Meall Horn and Beinn Aird da Loch salients, and the Stack of Glencoul.

primarily related to: 1) the decreasing quality of exposure of the mylonite section; 2) the increasingly smaller feldspar content of samples because mylonites in the footwall to Moine thrust are almost entirely derived from Cambrian quartzite rather than feldspar-rich Lewisian gneiss and; 3) increasing deformation temperatures that result in feldspar beginning to deform by crystal plasticity. Vorticity analysis of two mylonitic Cambrian quartzites yield W_m estimates ranging from 0.60 to 0.70 (58–50% pure shear), with arithmetic mean minimum ($W_m$min) and arithmetic mean maximum ($W_m$max) values of 0.62 (57% pure shear) and 0.69 (51% pure shear), respectively. W_m estimates obtained from 19 mylonitic Moine psammite samples from the Moine nappe range from 0.52 to 0.80 (64–40% pure shear), with $W_m$min and $W_m$max values of 0.59 (58% pure shear) and 0.67 (53% pure shear), respectively. At the Stack of Glencoul, Law (2010) reported rigid grain W_m estimates of 0.62–0.83 (57–37% pure shear; $W_m$min = 0.70, $W_m$max = 0.74) for six Moine samples located at 1 cm to 80 m above the ductile Moine thrust, and W_m estimates of 0.67–0.76 (53–44% pure shear; $W_m$min = 0.72, $W_m$max = 0.76) for six samples of mylonitic Cambrian quartzite at 0.5 cm to 13 m beneath the thrust.

8. Factors controlling vorticity and strain symmetry

8.1. Flow partitioning related to variations in thrust zone geometry and footwall structural architecture

To examine along strike variation of kinematic vorticity at the base of the Moine nappe and in the underlying mylonitic thrust sheets, we constructed a profile (Fig. 11) which displays vorticity values along strike from the Loch Dionard recess in the north to the Stack of Glencoul in the south. This along strike section represents the sampling interval with the greatest density of samples that were deemed appropriate for rigid grain vorticity analysis. W_m estimates of samples collected along the profile range from 0.53 to 0.80 (63–40% pure shear) in the Moine nappe and 0.52–0.83 (64–36% pure shear) in the underlying mylonitic thrust sheet(s). Our more limited vorticity data for the area along strike to the south collected exclusively from Moine mylonites between the Stack of Glencoul and Knockan are summarized in Fig. 12. W_m estimates of samples collected along this southern profile range from 0.52 to 0.60 (64–58% pure shear).

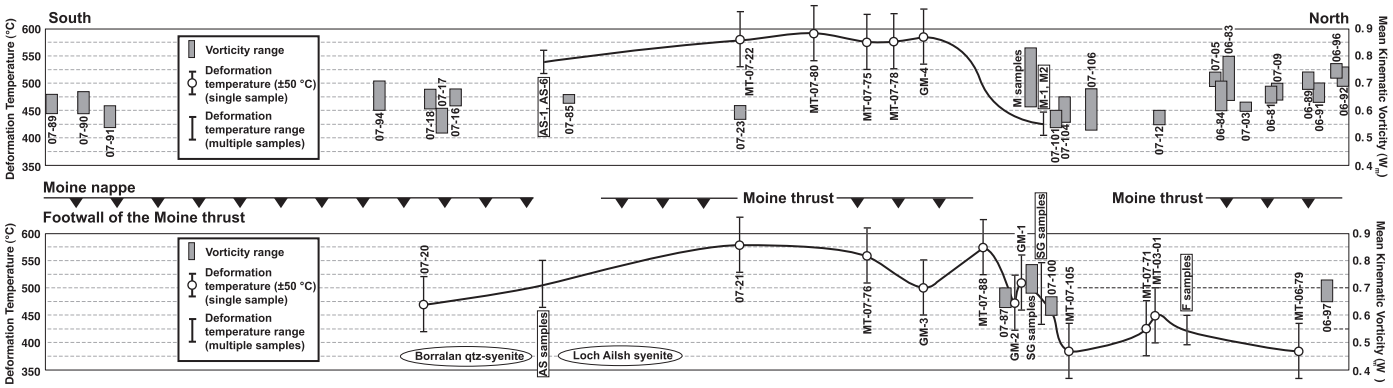

Fig. 12. Along strike vorticity and deformation temperature profile from Loch More (north end of profile) to Knockan Crag for the Moine and underlying mylonitic thrust sheets (where present/preserved). Sample locations in Fig. 2.

Along these transects, we focused on correlating flow partitioning with variation in structural depth (i.e. distance above and below the ductile Moine thrust) and footwall architecture of the underlying lower MTZ, as well as lithologic variation, which is limited. However, we emphasize that compared with published vorticity data from other orogenic belts, which have almost exclusively concentrated on individual vertical sampling transects, along-strike variability in W_m estimates for the Moine thrust mylonites is remarkably small (Figs. 11 and 13). Similarly, our rigid grain data indicate that estimated W_m values for samples from the base of the Moine nappe and underlying mylonitic thrust sheets at individual along strike positions are also remarkably similar (Figs. 11a and 12). We find the lack of along-strike variability in estimated W_m values based on these rigid grain data to be surprising, given both the considerable along strike variation in 3-D strain, variation in deformation temperature of these high strain rocks, and the variation in structural architecture of the underlying lower temperature parts of the MTZ. Previously reported analyses of these high strain rocks have concentrated on samples collected on individual vertical transects through the sequence of mylonites. For example, Law et al. (1986) and Law (1987) described a transition from asymmetric to symmetric quartz c- and a-axis fabrics beneath the ductile Moine thrust at the Stack of Glencoul that they attributed to strain-path partitioning. Fabrics adjacent to the thrust plane were originally interpreted to indicate plane strain conditions, while fabrics at 0.3–8.5 m beneath the thrust indicated general flattening strains. Later quantitative vorticity analyses using integrated strain and quartz c-axis fabric data documented a marked

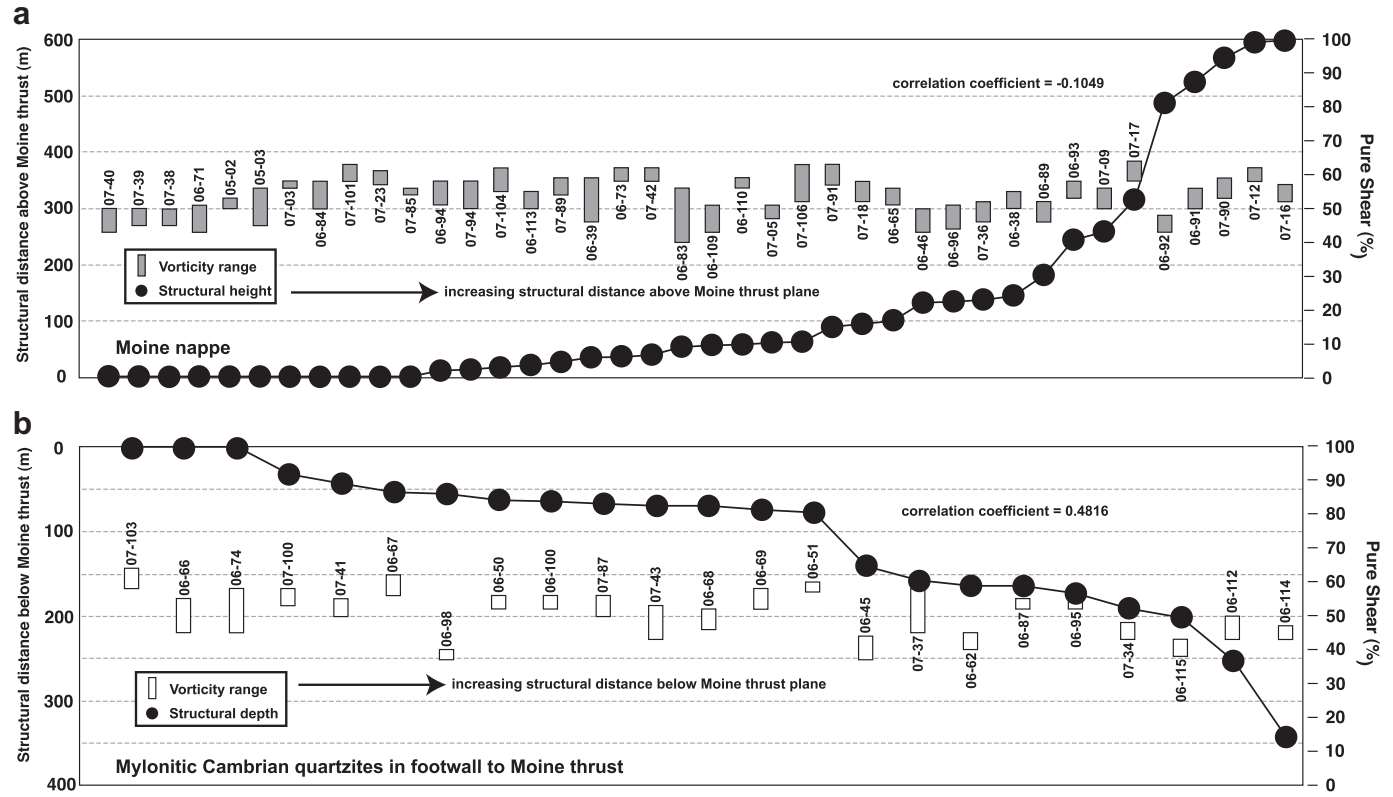

Fig. 13. (a) Structural height above Moine thrust plane vs. vorticity estimates for samples collected from the Moine nappe. (b) Structural depth beneath Moine thrust plane vs. vorticity estimates for samples collected from mylonitic thrust sheet(s) in footwall to Moine thrust. Samples in both plots are arranged with increasing structural distance from the thrust (to the right), and are not arranged with respect to geographic position.

increase in simple shear traced upward to the thrust plane, while vorticity analyses using rigid grain data from both hangingwall and footwall rocks indicated only minor increases in simple shear component traced toward the thrust plane (Law et al., 2007; Law, 2010). This result may indicate that rigid grain techniques provide some form of time-averaged estimate of flow vorticities and are insensitive to localized transient episodes of focused simple shearing, while techniques incorporating crystal-fabric data are particularly sensitive to the later episodes of flow due to fabric overprinting.

The MTZ from Loch Dionard south to the Stack of Glencoul exposes two salient-recess pairs – the Beinn Aird da Loch – Strath nan Aisinnin and Creagan Meall Horn – Loch Dionard salient-recess pairs (Fig. 11b), in addition to the major Assynt recess south of the Stack of Glencoul. Comparison of our vorticity data from these two salient-recess pairs (summarized in Fig. 11c) indicates that no significant deformation partitioning occurs along strike. This finding is in contradiction to Strine and Mitra (2004) who argued, based on strain and qualitative quartz fabric data, that significant kinematic differences exist between the Beinn Aird da Loch salient and the Strath nan Aisinnin recess (Fig. 11b). Within the recesses, footwall samples yield W_m estimates ranging from 0.65 to 0.82 (55–38% pure shear), with arithmetic mean minimum ($W_m$min) and mean maximum ($W_m$max) values of 0.70 and 0.77 (50% and 43% pure shear), respectively. W_m estimates of hangingwall samples from the recess range from 0.56 to 0.78 (62–43% pure shear), with a $W_m$min of 0.64 (56% pure shear) and a $W_m$max of 0.70 (50% pure shear). In the salients, W_m estimates of footwall samples range from 0.66 to 0.73 (54–47% pure shear), with a $W_m$min of 0.66 (54% pure shear) and a $W_m$max of 0.73 (47% pure shear), and hangingwall samples range from 0.55 to 0.78 (62–43% pure shear), with a $W_m$min of 0.63 (56% pure shear) and a $W_m$max of 0.71 (50% pure shear). These data suggest that formation of the salient-recess pairs is not due to lateral variations in flow vorticity in the Moine thrust zone mylonites. Of course it is also possible that the map pattern of salients and recesses is due to later brittle low angle thrusting that is unrelated to earlier flow within the mylonites.

8.2. Flow partitioning and structural depth

Numerous studies have recognized significant changes in W_m values with structural depth, and this variation has generally been interpreted as reflecting either distance from major thrust sheet-bounding faults (e.g. Xypolias and Kokkalas, 2006; Xypolias et al., 2010) or position (i.e. top vs. bottom) within the orogenic wedge (Jessup et al., 2006). To investigate possible links between flow partitioning and structural depth, we examined the relationship between W_m values and structural position in the Moine nappe and underlying mylonitic thrust sheet(s), relative to the local position of the intervening Moine thrust plane (Fig. 13).

Linear correlation coefficients of −0.1049 and 0.4816 were calculated for structural position vs. W_m in the Moine nappe and underlying mylonitic thrust sheet(s), respectively. The similarity of vorticity independent of structural position may be interpreted as indicating that flow was not partitioned across this 950 m sampling range. As discussed above for the Stack of Glencoul mylonites, however, it should be kept in mind that the rigid grain technique may be relatively insensitive to localized transient episodes of focused simple shearing, for example where sub-horizontal simple shearing occurs in a nappe sequence deforming by sub-vertical shortening with a significant pure shear component. The lack of documented vertical flow partitioning in our samples may also be a function of tectonic scale, with partitioning occurring on a larger vertical scale than can be appreciated in the limited vertical range of ~1 km. In the Himalaya, for example, Larson and Godin (2009), citing data from other studies (i.e. Grasemann et al., 1999; Law et al., 2004; Carosi et al., 2006; Jessup et al., 2006), have noted significant flow partitioning across the entire structural thickness (>30 km) of the Greater Himalayan Sequence. Similarly, working at a smaller scale, Xypolias and Kokkalas (2006, their Fig. 10b) have recognized significant variation of W_m across a structural depth profile of ~2000 m (W_m values of 0.10–1.00; 93–0% pure shear) in the External Hellenides.

8.3. Flow partitioning related to variation in deformation temperatures

Although we had hoped to be able to compare estimated deformation temperatures and vorticity values for a considerable number of samples covering a substantial along strike length of the Moine thrust mylonites, this strategy proved impossible for a number of reasons, including: 1) Lithologically, while quartzo-feldspathic psammite of the Moine nappe and Lewisian gneiss of the underlying mylonitic thrust sheet(s) are ideal for rigid grain vorticity analysis, rarely, however, are either of these units suitable for quartz petrofabric analyses, 2) While cross-girdle fabrics were measured in both mylonitic Cambrian quartzites below the Moine thrust and quartz-rich Moines above the thrust (Figs. 6–9), these tectonites generally have only a small feldspar content, thus limiting their applicability for rigid grain based techniques of vorticity analysis. With the data available (Fig. 12), no convincing correlation can be made between W_m values based on rigid grain data and estimated deformation temperatures.

9. Discussion and tectonic implications

9.1. Vertical ductile thinning

Wallis et al. (1993) have established numerical relationships that allow integration of strain magnitude and vorticity data to estimate the amount of shortening perpendicular to the flow plane in a general shear. In the MTZ mylonites we assume that the flow plane is oriented sub-parallel to the ductile Moine thrust plane and pervasive gently ESE dipping foliation. Although plane strain ($k = 1$) is assumed in the original numerical method of Wallis (1993), both 3-D strain analyses by Law et al. (2007, 2010) from the Stack of Glencoul mylonitic Cambrian quartzites, and the small circle pattern of quartz c- and a-axis fabrics produced in this study using EBSD, indicate that a general flattening deformation ($1 > k > 0$) must be taken in to account for the majority of the Moine thrust mylonites. Flattening strains inherently indicate extension along orogenic strike parallel to the *Y*-axis of the strain ellipsoid, unless compensated for by processes such as volume loss, and thus will decrease the amount of lineation parallel extension (extrusion) accordingly. Law et al. (2007) and Law (2010) proposed a graphical method to estimate changes in lineation parallel extrusion based on percentage stretch in the *Y*-direction. Although no quantitative strain estimates were obtained from the Assynt region in our study, integrated 3-D strain and vorticity data from the footwall of the Moine thrust at the Stack of Glencoul indicate 50–75% foliation-normal shortening depending on structural position and method of vorticity analysis employed (Law, 2010). Vorticity estimates and intensity of fabric development in the Stack of Glencoul mylonites are very similar to those reported here from other mylonite samples collected along strike at a similar structural level, both to the north and south of the Stack of Glencoul, in the Assynt region (Figs. 11 and 12; Tables 3 and 4). These combined data from the Moine thrust mylonites indicate that laterally widespread foliation

Table 3
Rigid grain vorticity estimates for Moine psammites in hangingwall to Moine thrust.

Sample	Min. W_m	Max. W_m	[a]BNGRS coordinates
MT-06-109	0.69	0.78	NC 38292 47376
MT-06-110	0.59	0.63	NC 38210 47105
MT-06-113	0.65	0.71	NC 37647 45680
MT-07-42	0.56	0.60	NC 36483 45458
MT-07-40	0.71	0.78	NC 35974 45189
MT-07-39	0.70	0.75	NC 35626 45339
MT-07-38	0.71	0.75	NC 35353 45501
MT-06-38	0.65	0.70	NC 34524 45688
MT-06-39	0.59	0.74	NC 34268 45301
MT-06-65	0.63	0.69	NC 34438 44864
MT-06-71	0.69	0.78	NC 33474 43757
MT-06-73	0.55	0.60	NC 33390 43548
MT-05-02	0.67	0.70	NC 33300 43440
MT-05-03	0.63	0.75	NC 33300 43440
MT-06-49	0.56	0.62	NC 33733 42737
MT-06-48	0.65	0.70	NC 33917 42728
MT-06-47	0.60	0.63	NC 34150 42695
MT-06-46	0.70	0.78	NC 33952 42387
MT-07-36	0.68	0.74	NC 33906 41502
MT-06-94	0.60	0.69	NC 32892 40238
MT-06-93	0.60	0.67	NC 33427 39630
MT-06-96	0.72	0.77	NC 32805 38864
MT-06-92	0.69	0.76	NC 33572 39002
MT-06-91	0.63	0.70	NC 33581 38124
MT-06-89	0.68	0.74	NC 33995 37254
MT-07-09	0.64	0.70	NC 32002 36765
MT-06-81	0.63	0.69	NC 32082 36500
MT-07-03	0.60	0.63	NC 32743 35315
MT-06-83	0.64	0.80	NC 33265 34501
MT-06-84	0.60	0.71	NC 33255 34226
MT-07-05	0.69	0.74	NC 33351 33943
MT-07-12	0.55	0.60	NC 33372 31389
MT-07-106	0.53	0.68	NC 29625 30380
MT-07-104	0.56	0.65	NC 29000 29595
MT-07-101	0.54	0.60	NC 29350 28910
[b]M-1	0.75	0.83	NC 28880 28760
[b]M-2	0.74	0.77	NC 28880 28760
[b]M-3	0.62	0.70	NC 28930 28680
[b]M-4	0.73	0.75	NC 28930 28680
[b]M-5	0.73	0.77	NC 28930 28680
[b]M-6	0.73	0.77	NC 28930 28680
MT-07-23	0.57	0.62	NC 35097 17449
MT-07-85	0.63	0.66	NC 32270 11241
MT-07-16	0.62	0.68	NC 30460 07040
MT-07-17	0.52	0.61	NC 30240 06501
MT-07-18	0.61	0.68	NC 29666 06338
MT-07-94	0.60	0.71	NC 28025 05550
MT-07-91	0.54	0.62	NC 18395 07540
MT-07-90	0.59	0.67	NC 17795 06600
MT-07-89	0.59	0.66	NC 16909 05617

[a] British National Grid Reference System.
[b] Samples from Law (in press).

Table 4
Rigidgrain vorticity estimates for samples collected in the footwall of the Moine thrust.

Sample No	Unit/Lithology	Min. W_m	Max. W_m	[a]BNGRS coordinates
MT-06-115	Lewisian	0.77	0.82	NC 37327 46522
MT-06-114	Lewisian	0.73	0.78	NC 37456 46125
MT-06-112	Lewisian	0.70	0.77	NC 37507 46057
MT-07-43	Lewisian	0.67	0.78	NC 36716 45781
MT-07-41	Lewisian	0.65	0.71	NC 36200 45375
MT-07-37	Lewisian	0.60	0.75	NC 35307 45646
MT-06-103	Lewisian	0.52	0.60	NC 34849 43902
MT-06-100	Lewisian	0.63	0.68	NC 34677 46065
MT-06-98	Lewisian	0.80	0.83	NC 34676 46080
MT-06-87	Lewisian -ultramylonite	0.65	0.68	NC 34275 46100
MT-06-62	Lewisian	0.75	0.80	NC 34124 45248
MT-06-66	Lewisian	0.65	0.75	NC 34278 44561
MT-06-67	Lewisian	0.55	0.64	NC 33927 44323
MT-06-68	Lewisian	0.68	0.74	NC 33780 44259
MT-06-69	Lewisian	0.61	0.68	NC 33696 44131
MT-06-74	Lewisian	0.60	0.75	NC 33234 43386
MT-06-51	Lewisian	0.58	0.62	NC 33194 43139
MT-06-50	Lewisian	0.64	0.68	NC 33298 43036
MT-07-34	Lewisian	0.72	0.77	NC 33859 41842
MT-06-45	Lewisian	0.76	0.83	NC 33742 41856
MT-06-95	Lewisian	0.62	0.68	NC 32638 39886
MT-06-97	Lewisian	0.65	0.73	NC 32870 38405
MT-07-100	Cambrian quartzite	0.60	0.67	NC 29555 28600
[b]SG-1	Cambrian quartzite	0.75	0.78	NC 28880 28700
[b]SG-2.4	Cambrian quartzite	0.67	0.74	NC 28880 28763
[b]SG-8	Cambrian quartzite	0.72	0.76	NC 28930 28680
[b]SG-9	Cambrian quartzite	0.72	0.74	NC 28930 28680
[b]SG-10	Cambrian quartzite	0.68	0.72	NC 28880 28760
[b]SG-13	Cambrian quartzite	0.68	0.70	NC 28930 28680
MT-07-87	Cambrian quartzite	0.63	0.70	NC 30907 26456

[a] British National Grid Reference System.
[b] Samples from Law (in press).

normal vertical thinning must have occurred beneath the Moine nappe in the Assynt region.

9.1.1. Preservation of inverted metamorphic isograds

Perhaps one of the most important attributes of vertical ductile thinning is the preservation of inverted metamorphic isograds during progessive nappe stacking (Ring and Kassem, 2007). In the Scandian wedge of northern Scotland a progressive decrease in metamorphic grade is observed from the high P–T (11–12 kbar at 650–700 °C; Friend et al., 2000) migmatites of the Naver nappe to lower-amphibolite to greenschist facies rocks at the base of the Moine nappe and upper MTZ (Fig. 1). Although the mechanism(s) by which this isograd geometry was produced remains elusive, it was probably at least partially caused by thrusting (see discussion by Johnson and Strachan, 2006). Thrusting of higher grade thrust sheets over those of lower grade should lead to prograde metamorphism of the underlying thrust sheet, which is not observed in the Scandian nappe stack. One tectonic mechanism for preserving inverted isograds is pure shear driven vertical ductile thinning leading to synkinematic exhumation of the overriding higher grade thrust sheets, which may prevent heating of the structurally lower rocks. If syn-thrusting vertical ductile thinning occurred, as indicated by integrated strain and vorticity estimates, then P–T–t paths should indicate decompression following thrusting. Immediately beneath the Naver thrust, intense middle- to lower-amphibolite facies metamorphism occurred coeval with southeast-directed ductile oblique extension (Moorhouse and Moorhouse, 1988; Burns, 1994). Plagioclase moat textures developed between garnet and matrix phases in the Naver nappe indicate a decompression event and plagioclase-garnet thermobarometry yield P–T conditions of ~10 kbars at ~650 °C and 7–8 kbars at ~600 °C (Friend et al., 2000). Microstuctural relationships associated with these decompression textures indicate that they are syn to post Scandian thrusting.

9.1.2. Contribution of vertical ductile thinning to exhumation

Feehan and Brandon (1999) have examined the potential contribution made by vertical ductile thinning to total exhumation in a collisional orogenic wedge that grows by accretion of thrust sheets to the basal portions of the wedge. In their simplest one-dimensional numerical model, exhumation is controlled only by sub-vertical ductile thinning. In this case, however, for a material point, initially located at depth z within the wedge, to eventually reach the topographic surface, vertical ductile thinning would have to be 100%, which is obviously impossible. Thus, complete exhumation cannot occur by ductile thinning alone. When exhumation is increasingly controlled by other mechanisms, including erosion

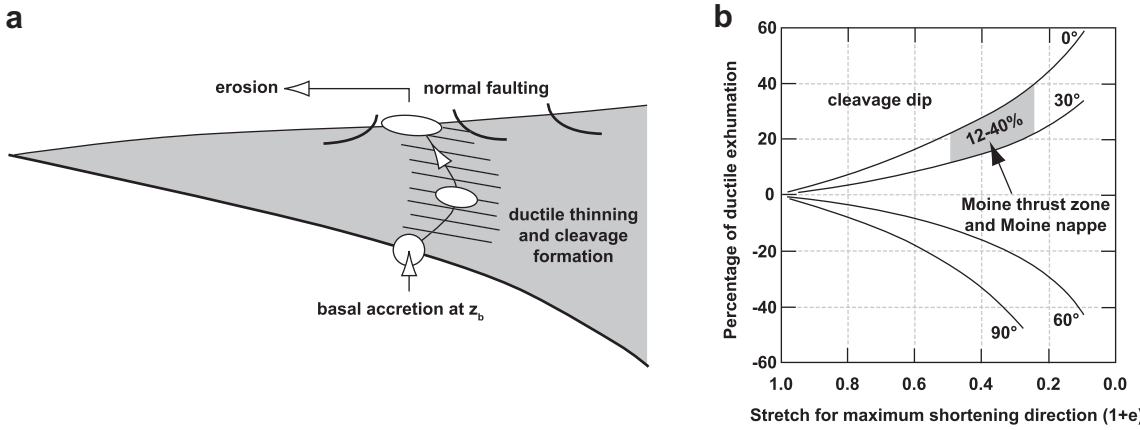

Fig. 14. (a) Model cross-section of a steady-state orogenic wedge showing the major variables that control thickening or thinning of the wedge. Flow path of exhumed particle of interest is shown. Modified from Feehan and Brandon (1999). (b) One dimensional plane strain exhumation model of Feehan and Brandon (1999) that assumes isochoric conditions, with gray area indicating data from mylonitic Cambrian quartzites at Stack of Glencoul. Input parameters of cleavage dip (0–30°) and stretch (0.50–0.25) for maximum foliation-normal shortening indicate a 12–40% contribution of vertical ductile thinning to total exhumation at the base of the Moine nappe.

and normal faulting, ductile thinning contributes progressively less to the overall material exhumation, and consequently each increment of vertical strain is distributed over a thinner section of overburden (Feehan and Brandon, 1999). In a more complex model that incorporates ductile thinning, erosion, and normal faulting, Feehan and Brandon (1999) suggested that the contribution of ductile thinning to the total exhumation can be assessed by determining the time-depth history of a particle of interest and assuming a steady-state wedge (erosion = basal accretion; Fig. 14a). As outlined above, Law (2010) has calculated vertical shortening values of 50–75% (equivalent to $1 + e_3$ values of 0.5–0.25) for the mylonitic Cambrian quartzites exposed at the Stack of Glencoul. By integrating these vertical shortening estimates into the Feehan and Brandon (1999) isochoric model, and in-putting the average dip of foliation of the MTZ mylonites and overlying Moine nappe (10–25°), the vertical ductile thinning contribution to total exhumation is estimated at 12–40% (Fig. 14b).

9.2. Linking upper- and lower-mid-crustal deformation processes

Vertical ductile thinning within the ductile regime must be accommodated by either volume loss or extrusion of material toward the synorogenic topographic surface. In the absence of significant volume loss, this vertical thinning requires considerable transport-parallel lengthening of thrust sheets. Therefore, the geometric consequences of transport-parallel thrust sheet stretching must be incorporated into models for the evolution of orogenic wedges in which vertical thinning and general shear are important. Numerous models have been proposed to explain mid-crustal transport-parallel flow of material in orogenic systems (e.g. Northrup, 1996; Vannay and Grasemann, 2001; Godin et al., 2006). If extrusion occurs toward the synorogenic topographic surface during collisional orogenesis, then by necessity a causal kinematic link exists between upper and lower crustal processes (Northrup, 1996). Firstly, displacement of material toward the topographic surface via lateral ductile flow must be transferred to discrete brittle structures above the ductile-brittle transition (Fig. 15). This tectonic linkage may have major implications for increasing strain rates and deformation mechanisms occurring at higher crustal levels traced toward the foreland (Williams et al., 2006). If significant components of both ductile flow and brittle displacement occurred along a single crustal-scale shear zone/thrust fault, examination of an upper to lower crustal profile should indicate a progressive change in deformation conditions/temperatures and microstructural styles. Secondly, along strike variations in extrusive flow at mid-crustal levels could be responsible for observed variations in displacement associated with brittle faulting and folding occurring in the foreland parts of orogenic systems. Finally, strain compatibility requires that upper crustal deformation above laterally flowing ductile material must either be decoupled from lower- to mid-crustal deformation (e.g. stretching fault, Means, 1989), or must also be in extension during flow of the underlying material (Fig. 15). As suggested by Vannay and Grasemann (2001) and Law et al. (2004), the South Tibetan Detachment system defining the top of the Greater Himalayan Slab is arguably the type example of this phenomenon. No such normal fault system has yet been identified in the Scandian orogenic wedge of northern Scotland, although the mounting evidence for general shear at the base of the Moine nappe would seem to require either a discreet normal fault or a broad zone of normal sense shear at some position within the overlying nappe pile.

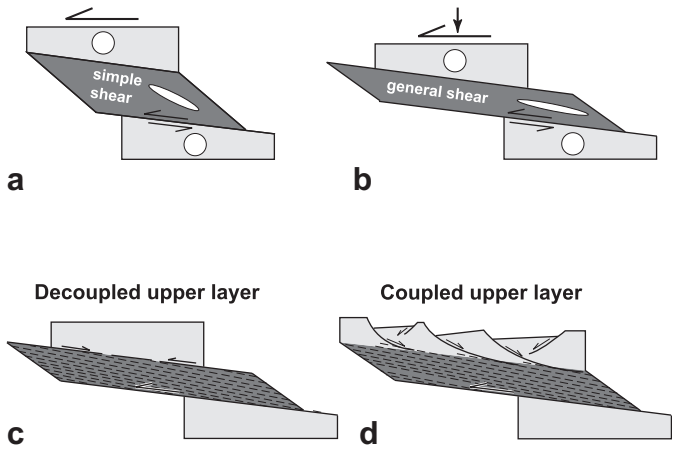

Fig. 15. Schematic models for mid-crustal flow associated with either simple shear (a) or general shear (b–d); modified from Northrup (1996).

10. Conclusions

Rigid grain vorticity analysis of samples collected along strike in the upper MTZ and overlying Moine nappe indicate that Scandian

thrusting involved a considerable pure shear component (64–37%) of penetrative deformation associated with vertical thinning. Although minor variability in W_m values is recognized along strike, these fluctuations cannot be directly correlated with changes in footwall structural architecture, lithology, deformation temperatures, or structural depth. Quartz c- and a-axis fabrics from mylonitic Cambrian quartzites in the immediate footwall to the Moine thrust indicate general flattening ($1 > k > 0$) strains, although locally more constrictional fabrics are also recorded adjacent to transport-parallel features such as the Oykel Transverse Zone in the overlying Moine nappe. These results are in agreement with 3-D strain estimates of mylonitic quartzites from the Stack of Glencoul (Law et al. 2010) and from Loch Eriboll to the north (Dayan, 1981; Law et al., 1984). In the overlying Moine nappe, quartz c-axis fabrics are generally characterized by asymmetric (top-to-the-west-northwest) single and cross-girdles, and their complimentary a-axis fabrics suggest that approximately plane strain non-coaxial deformation conditions were prevalent. Our combined evidence for general flattening and significant pure shear deformation suggests that foliation-normal shortening was accommodated by non-plane strike-orthogonal (i.e. transport-parallel) and strike-parallel ductile flow. Given the shallow dip (<20°) of the foliation, it is likely that flow was driven both toward the synorogenic topographic surface and along orogenic strike. Transport-parallel lengthening of 40–200% and along-strike stretching of 28–49% is indicated by integration of vorticity estimates and 3-D strain data for the Stack of Glencoul mylonites (Law et al., 2007; Law, 2010).

In the footwall to the Moine thrust, deformation temperatures estimated from quartz c-axis opening angles range from 380 to 580 °C, with the lowest and highest temperature estimates observed in northern Assynt and eastern Assynt, respectively. Deformation temperatures based on quartz c-axis opening angles in the overlying Moine nappe range from 520 to 585 °C, but our data are currently limited to the area between the Stack of Glencoul and the Loch Ailsh intrusive complex. The progressive apparent increase of deformation temperatures traced from north to southeast could indicate: 1) exhumation from structurally deeper levels in the southeast which, in turn would indicate greater displacement magnitudes along the southeastern sections of the Moine thrust or, 2) heat transfer from the Loch Ailsh alkaline intrusive complex and related suite of nordmarkite sills during thrusting and mylonite formation (Law and Johnson, 2010). Good agreement is found within all samples analyzed between deformation temperatures indicated by fabric opening angle and deformation temperature ranges indicated by quartz recrystallization regime. Nonetheless these deformation temperatures intuitively seem too high for mylonites that have traditionally been regarded as forming under low greenschist facies conditions. As both fabric opening angles and recrystallization regimes are sensitive to hydrolytic weakening and strain rate, as well as deformation temperature, application of a thermometer that is insensitive to these variables is urgently needed to test our inferred deformation temperatures.

Integrated 3-D strain and vorticity estimates from the Moine thrust footwall at the Stack of Glencoul indicate a 50–75% subvertical shortening, with estimated values depending on structural position and method of vorticity analysis employed (Law, 2010). Although we place little faith in the precise shortening amounts estimated, we interpret these results to indicate that considerable foliation-normal shortening must have occurred during mylonite generation beneath the Moine nappe. Our data indicate that this shortening must have laterally (i.e. along orogenic strike) been of regional extent. If vertical thinning of the Scandian orogenic wedge did occur, then some component of exhumation, and hence decompression, should be recorded in the nappe pile. Structurally above the Moine nappe, P–T analyses and metamorphic relations indicate a decompression event that is constrained to have occurred during Scandian (D_2) age thrusting (Friend et al., 2000). A lack of suitable mineral assemblages that could be used to provide robust P–T analyses has, to date, hindered the search for a comparable P–T history in the Moine nappe. Vertical ductile thinning must be accommodated by either volume loss or extrusion of material toward the synorogenic topographic surface. Extrusion toward the synorogenic topographic surface implies that upper and lower crustal processes must be somehow linked and such linkage presents significant implications for both the kinematic/geometric evolution of the Scandian orogenic wedge, and for the evolution of fault rocks within the wedge as displacement rates should increase on individual faults traced toward the foreland during the extrusion process (Williams et al., 2006).

Acknowledgements

The authors would like to thank Rob Butler, Rob Strachan, Bob Holdsworth, and the late Martin Casey for invaluable discussion on various of aspects of Northwest Scotland geology. Robert Marshall is acknowledged for preparation of EBSD samples at Leeds University. This work was funded by NSF grant EAR 0538031 to RDL and the VT Geosciences Byron Nelson Cooper Memorial Graduate Fellowship and Wallace D. Lowry Endowed Graduate Scholarship to JRT. Insightful and constructive reviews by Bill Sullivan and Kyle Larson and editor Bill Dunne significantly improved previous versions of this manuscript and are gratefully acknowledged.

Appendix. Supporting material

Supporting material associated with this article can be found in the online version, at doi:10.1016/j.jsg.2010.05.001.

References

Bailey, E.B., 1955. Moine tectonics and metamorphism in Skye. Transactions of the Edinburgh Geological Society 16, 93–166.
Bailey, C.M., Polvi, L.E., Forte, A.M., 2007. Pure shear dominated high-strain zones in basement terranes. In: Hatcher Jr., R.D., Carlson, M.P., McBride, J.H., Martínez Catalán, J.R. (Eds.), 4-D Framework of Continental Crust. Geological Society of America, pp. 93–108. Memoir, 200.
Bailey, E.B., McCallien, W.J., 1934. Precambrian Association excursion to Scotland. Geological Magazine 71, 553–555.
van Breemen, O., Aftalion, M., Johnson, M.R.W., 1979. Age of the Loch Borrolan complex, Assynt, and the late movements along the Moine thrust zone. Journal of the Geological Society, London 136, 489–496.
British Geological Survey, 2002. Loch Eriboll, Scotland Sheet 114W, Solid Geology, 1:50 000, Provisional Series. British Geological Survey, Keyworth, Nottingham.
British Geological Survey, 2007. Assynt, Scotland Special Sheet, Bedrock, 1:50 000 Geology Series. British Geological Survey, Keyworth, Nottingham.
British Geological Survey, 2009. Ben Hee, Scotland Sheet 108W, Solid Geology, 1:50 000 Geology Series. British Geological Survey, Keyworth, Nottingham.
Burns, I.M., 1994. Tectonothermal Evolution and Petrogenesis of the Naver and Kirtomy Nappes, North Sutherland, Scotland. Ph.D. Thesis, Oxford Brookes University.
Carosi, R., Montomoli, C., Rubatto, D., Visona, D., 2006. Normal-sense shear zones in the core of the Higher Himalayan Crystallines (Bhutan Himalayas): evidence for extrusion? In: Law, R.D., Butler, R.W.H., Holdsworth, R., Krabbendam, M., Strachan, R. (Eds.), Channel Flow, Extrusion, and Exhumation in Continental Collision Zones Geological Society, London Special Publications 335.
Chapple, W.M., 1978. Mechanics of thin-skinned fold-and-thrust belts. Geological Society of America Bulletin 89, 1189–1198.
Cheer, D.A., 2006. The Sedimentary, Structural, and Igneous Geology of the Moine Thrust Zone and Moine Nappe in the Ben Hee Area, NW Scotland. Ph.D. Thesis, University of St. Andrews.
Cutts, K.A., Hand, M., Kelsey, D.E., Strachan, R.A., 2009. Orogenic versus extensional setting for regional metamorphism: Knoydartian events in the Moine Supergroup revisted. Journal of the Geological Society, London 166, 201–204.
Dahlen, F.A., 1990. Critical taper model of fold-and-thrust belts and accretionary wedges. Annual Review of Earth and Planetary Sciences 18, 55–99.
Dahlen, F.A., Suppe, J., Davis, D., 1984. Mechanics of fold-and-thrust belts and accretionary wedges: Cohesive Couloumb theory. Journal of Geophysical Research 89, 10087–10101.

Dallmeyer, D., Strachan, R.D., Rogers, G., Watt, G.R., Friend, C.R.L., 2001. Dating deformation and cooling in the Caledonian thrust nappes of north Sutherland, Scotland: insights from $^{40}Ar/^{39}Ar$ and Rb–Sr chronology. Journal of the Geological Society, London 158, 501–512.

Davis, D., Suppe, J., Dahlen, F.A., 1983. Mechanics of fold-and-thrust belts and accretionary wedges. Journal of Geophysical Research 88, 1153–1172.

Dayan, H., 1981. Deformation Studies of the Folded Mylonites of the Moine Thrust, Eriboll District, Northwest Scotland. Ph.D. Thesis, University of Leeds.

Elliott, D., Johnson, M.R.W., 1980. The structural evolution of the northern part of the Moine thrust zone. Transactions of the Royal Society of Edinburgh: Earth Sciences 71, 69–96.

Feehan, J.G., Brandon, M.T., 1999. Contribution of ductile flow to exhumation of low-temperature, high-pressure metamorphic rocks: San Juan-Cascade nappes, NW Washington State. Journal of Geophysical Research 104, 10883–10902.

Freeman, S.R., Butler, R.W.H., Cliff, R.A., Rex, D.C., 1998. Direct dating of mylonite evolution: a multidisciplinary geochronological study from the Moine thrust zone, NW Scotland. Journal of the Geological Society, London 155, 745–758.

Friend, C.R.L., Jones, K.A., Burns, I.M., 2000. New high-pressure event in the Moine Supergroup, northern Scotland: implications for Taconic (early Caledonian) crustal evolution. Geology 28, 543–546.

Geological Survey of Great Britain (Scotland), 1923. Geological Map of the Assynt District at 1:63,360. Geological Survey of Great Britain, Scotland.

Godin, L., Grujic, D., Law, R.D., Searle, M.P., 2006. Channel flow, ductile extrusion and exhumation in continental collision zones: an introduction. In: Law, R.D., Searle, M.P., Godin, L. (Eds.), Channel Flow, Ductile Extrusion and Exhumation in Continental Collision Zones. Geological Society London, pp. 1–23. Special Publications, 268.

Goodenough, K.M., Evans, J.A., Krabbendam, M., 2006. Constraining the maximum age of movements in the Moine thrust belt: dating the Canisp Porphyry. Scottish Journal of Geology 42, 77–81.

Grasemann, B., Fritz, H., Vannay, J.-C., 1999. Quantitative kinematic flow analysis from the Main Central Thrust zone, (NW Himalaya): implications for a decelerating strain path and the extrusion of orogenic wedges. Journal of Structural Geology 21, 837–853.

Halliday, A.N., Aftalion, M., Parsons, I., Dickin, A.P., Johnson, M.R.W., 1987. Syn-orogenic alkaline magmatism and its relationship to the Moine Thrust Zone and the thermal state of the lithosphere in Northwest Scotland. Journal of the Geological Society, London 144, 611–617.

Holdsworth, R.E., Strachan, R.A., Alsop, G.I., 2001. Geology of the Tongue District. In: Memoir of the British Geological Survey. HMSO.

Holdsworth, R.E., Strachan, R.A., Alsop, G.I., Grant, C.J., Wilson, R.W., 2006. Thrust sequences and the significance of low-angle, out-of-sequence faults in the northernmost Moine Nappe and Moine Thrust zone, NW Scotland. Journal of the Geological Society, London 163, 801–814.

Holdsworth, R.E., Alsop, G.I., Strachan, R.A., 2007. Tectonic stratigraphy and structural continuity of the northernmost Moine thrust zone and Moine nappe, Scottish Caledonides. In: Ries, A.C., Butler, R.W.H., Graham, R.H. (Eds.), Deformation of the Continental Crust: The Legacy of Mike Coward. Geological Society, London, pp. 121–142. Special Publications 272.

Holdsworth, R.E., Grant, C.J., 1990. Convergence-related 'dynamic spreading' in a mid-crustal ductile thrust zone: a possible orogenic wedge model. In: Knipe, R.J., Rutter, E.H. (Eds.), Deformation, Rheology and Tectonics. Geological Society, London, pp. 491–500. Special Publications 54.

Jessup, M., Law, R.D., Searle, M.P., Hubbard, M., 2006. Structural evolution and vorticity of flow during extrusion and exhumation of the Greater Himalayan Slab, Mount Everest Massif, Tibet/Nepal: implications for orogen-scale flow partitioning. In: Law, R.D., Searle, M.P., Godin, L. (Eds.), Channel Flow, Ductile Extrusion and Exhumation in Continental Collision Zones. Geological Society London, pp. 379–413. Special Publications 268.

Jessup, M.J., Law, R.D., Frassi, C., 2007. The Rigid Grain Net (RGN): an alternate method for estimating mean kinematic vorticity number (Wm). Journal of Structural Geology 29, 411–421.

Johnson, M.R.W., Kelly, S.P., Oliver, G.J.H., Winter, D.A., 1985. Thermal effects and timing of thrusting in the Moine thrust zone. Journal of the Geological Society, London 142, 863–874.

Johnson, M.R.W., Strachan, R., 2006. A discussion of possible heat sources during nappe stacking: the origin of Barrovian metamorphism within the Caledonian sheets of NW Scotland. Journal of the Geological Society, London 163, 579–582.

Kassem, M.K., Ring, U., 2004. Underplating-related finite-strain patterns in the Gran Paradiso Massif, Italian Western Alps. Heterogeneous ductile strain superimposed on a nappe stack. Journal of the Geological Society, London 161, 875–884.

Kidder, S., Ducea, M.N., 2006. High temperatures and inverted metamorphism in the schist of Sierra de Salinas, California. Earth and Planetary Science Letters 240, 422–437.

Knipe, R.J., 1990. Microstructural analysis and tectonic evolution in thrust systems: examples from the Assynt region of the Moine Thrust Zone, Scotland. In: Barber, D.J., Meredith, P.G. (Eds.), Deformation Processes in Minerals, Ceramics and Rocks. Mineralogical Society of Great Britain and Ireland. Unwin Hyman, London, pp. 228–261.

Kohn, M.J., Northrup, C.J., 2009. Taking mylonites' temperatures. Geology 37, 47–50.

Krabbendam, M., Prave, T., Cheer, D., 2008. A fluvial origin for the Neoproterozoic Morar Group, NW Scotland: implications for Torridon-Morar Group correlation and the Grenville orogen foreland basin. Journal of the Geological Society, London 165, 379–394.

Kruhl, J.H., 1998. Reply: prism- and basal-plane parallel subgrain boundaries in quartz: a microstructural geothermobarometer. Journal of Metamorphic Geology 16, 142–146.

Larson, K.P., Godin, L., 2009. Kinematics of the greater Himalayan sequence, Dhaulagiri Himal: implications for the structural framework of central Nepal. Journal of the Geological Society, London 166, 25–44.

Law, R.D., 1986. Relationships between strain and quartz crystallographic fabrics in the Roche Maurice quartzites of Plougastel, western Brittany. Journal of Structural Geology 8, 493–515.

Law, R.D., 1987. Heterogenous deformation and quartz crystallographic fabric transitions: natural examples from the Moine thrust zone at the Stack of Glencoul, northern Assynt. Journal of Structural Geology 9, 819–833.

Law, R.D., 1990. Crystallographic fabrics: a selective review of their applications to research in structural geology. In: Knipe, R.J., Rutter, E.H. (Eds.), Deformation Mechanisms, Rheology and Tectonics. Geological Society, London, pp. 335–352. Special Publications 54.

Law, R.D., Knipe, R.J., Dayan, H., 1984. Strain path partitioning within thrust sheets; microstructural and petrofabric evidence from the Moine thrust zone at Loch Eriboll, Northwest Scotland. Journal of Structural Geology 6, 477–497.

Law, R.D., Casey, M., Knipe, R.J., 1986. Kinematic and tectonic significance of microstructures and crystallographic fabrics within quartz mylonites from the Assynt and Eriboll regions of the Moine thrust zone, NW Scotland. Transactions of the Royal Society of Edinburgh: Earth Sciences 77, 99–123.

Law, R.D., Searle, M.P., Simpson, R.L., 2004. Strain, deformation temperatures and vorticity of flow at the top of the greater Himalayan Slab, Everest Massif, Tibet. Journal of the Geological Society, London 161, 305–320.

Law, R.D., Thigpen, J.R., Cook, B., 2007. Field excursion C – mylonites associated with the stack of Glencoul: May 15th and 17th 2007. In: Strachan, R., Thigpen, J.R. (Eds.), Continental Tectonics and Mountain Building – the Peach and Horne Meeting. A Guide to Field Excursions, pp. 66–103. Joint meeting of the Geological Society of London (an Arthur Holmes meeting) and Geological Society of America to celebrate the centenary of the Peach and Horne 1907 Geological Survey of Scotland memoir on "The Geological Structure of the Northwest Highlands of Scotland", Ullapool, Scotland, 12–19 May 2007.

Law, R.D., Mainprice, D.H., Casey, M., Lloyd, G.E., Knipe, R.J., Cook, B., Thigpen, J.R., 2010. Moine thrust zone mylonites at the stack of Glencoul I – microstructures, strain and influence of recrystallization on quartz crystal fabric development. In: Law, R.D., Butler, R.W.H., Holdsworth, R., Krabbendam, M., Strachan, R. (Eds), Continental Tectonics and Mountain Building – The Legacy of Peach and Horne. Geological Society, London, Special Publications 335, 543–577.

Law, R.D., Johnson, M.R.W., 2010. Microstructures and crystal fabrics of the Moine thrust zone and Moine nappe: history of research and changing tectonic interpretations. In: Law, R.D., Butler, R.W.H., Holdsworth, R., Krabbendam, M., Strachan, R. (Eds), Continental Tectonics and Mountain Building – The Legacy of Peach and Horne. Geological Society, London, Special Publications 335, 443–503.

Law, R.D., 2010. Moine thrust zone mylonites at the stack of Glencoul II: results of vorticity analyses and their tectonic significance. In: Law, R.D., Butler, R.W.H., Holdsworth, R., Krabbendam, M., Strachan, R. (Eds), Continental Tectonics and Mountain Building – The Legacy of Peach and Horne. Geological Society, London, Special Publications 335, 579–602.

Law, R.D., 2010. Moine thrust zone mylonites at the stack of Glencoul II: results of vorticity analyses and their tectonic significance. In: Law, R.D., Butler, R.W.H., Holdsworth, R., Krabbendam, M., Strachan, R. (Eds), Continental Tectonics and Mountain Building – The Legacy of Peach and Horne. Geological Society, London, Special Publications 335, 359–381.

Lister, G.S., 1977. Discussion: crossed-girdle c-axis fabrics in quartzites plastically deformed by plane strain and progressive simple shear. Tectonophysics 39, 51–54.

Lister, G.S., Dornsiepen, U.F., 1982. Fabric transitions in the Saxony Granulite Terrain. Journal of Structural Geology 4, 81–92.

Lister, G.S., Paterson, M.S., Hobbs, B.E., 1978. The simulation of fabric development in plastic deformation and its application to quartzite: the model. Tectonophysics 45, 107–158.

Lister, G.S., Hobbs, B.E., 1980. The simulation of fabric development during plastic deformation and its application to quartzite: the influence of deformation history. Journal of Structural Geology 2, 355–371.

MacGregor, A.G., 1952. Metamorphism of the Moine nappe in northern Scotland. Transactions of the Edinburgh Geological Society 15, 241–257.

Means, W.D., 1989. Stretching faults. Geology 17, 893–896.

Mendum, J.R., Barber, A.J., Butler, R.W.H., Flinn, D., Goodenough, K.M., Krabbendam, M., Park, R.G., Stewart, A.D. (Eds.), 2009. Lewisian, Torridonian and Moine Rocks of Scotland. Geological Conservation Review Series. Joint Nature Conservation Committee, Peterborough, p. 721.

Moorhouse, S.J., Moorhouse, V.E., 1988. The Moine assemblage in Sutherland. In: Winchester, J.A. (Ed.), Later Proterozoic Stratigraphy in the Northern Atlantic Regions. Blackie, Glasgow, pp. 54–73.

Morgan, S.S., Law, R.D., 2004. Unusual transition in quartzite dislocation creep regimes and crystal slip systems in the aureole of the Eureka Valley-Joshua Flat-Beer Creek Pluton, California: a case for anhydrous conditions created by decarbonation reactions. Tectonophysics 384, 209–231.

Northrup, C.J., 1996. Structural expressions and tectonic implications of general noncoaxial flow in the midcrust of a collisional orogen: the Scandinavian Caledonides. Tectonics 15, 490–505.

Passchier, C.W., 1987. Stable positions of rigid objects in non-coaxial flow – a study in vorticity analysis. Journal of Structural Geology 9, 679–690.
Passchier, C.W., Trouw, R.A.J., 2005. Micro-tectonics, second ed. Springer, 366 pp.
Peach, B.N., Horne, J., Gunn, W., Clough, C.T., Hinxman, L.W., Cadell, H.M., 1888. Report on recent work of the Geological Survey in the N.W. Highlands of Scotland, based on field notes and maps. Quarterly Journal of the Geological Society, London 64, 378–441.
Peach, B.N., Horne, J., Gunn, W., Clough, C.T., Hinxman, L.W., Teall, J.J.H., 1907. The Geological Structure of the North-West Highlands of Scotland. In: Memoir of the Geological Survey of Great Britain.
Platt, J.P., 1986. Dynamics of orogenic wedges and the uplift of high pressure metamorphic rocks. Geological Society of America Bulletin 97, 1037–1953.
Price, J.P., 1985. Preferred orientations in quartzites. In: Wenk, H.R. (Ed.), Preferred Orientations in Deformation Metals and Rocks: An Introduction to Modern Texture Analysis. Academic Press, pp. 85–406.
Read, H.H., 1931. The Geology of Central Sutherland (Sheets 108 and 109). In: British Geological Survey Memoir, 238 pp.
Ring, U., Kassem, M.K., 2007. The nappe rule: why does it work? Journal of the Geological Society, London 164, 1109–1112.
Schmid, S.M., Casey, M., 1986. Complete fabric analysis of some commonly observed quartz c-axis patterns. In: Hobbs, B.E., Heard, H.C. (Eds.), Mineral and Rock Deformation Laboratory Studies: The Paterson Volume. Geophysical Monograph 36. American Geophysical Union, pp. 263–286.
Searle, M.P., Law, R.D., Dewey, J.F., Streule, M.J., 2010. Relationships between the Loch Ailsh and Borralan alkaline intrusions and thrusting in the Moine thrust zone, southern Assynt culmination, NW Scotland. In: Law, R.D., Butler, R.W.H., Holdsworth, R., Krabbendam, M., Strachan, R. (Eds), Continental Tectonics and Mountain Building – The Legacy of Peach and Horne. Geological Society, London, Special Publications 335, 383–404.
Stephenson, B.J., Waters, D.J., Searle, M.P., 2000. Inverted metamorphism and the Main central thrust: field relations and thermobarometric constraints from the Kishtwar Window, NW Indian Himalaya. Journal of Metamorphic Geology 18, 571–590.
Stipp, M., Stunitz, H., Heilbronner, R., Schmid, S.M., 2002a. The eastern Tonale fault zone; a "natural laboratory" for crystal plastic deformation of quartz over a temperature range from 250 to 700 °C. Journal of Structural Geology 24, 1861–1884.
Stipp, M., Stunitz, H., Heilbronner, R., Schmid, S., 2002b. Dynamic recrystallization of quartz: correlation between natural and experimental conditions. In: De Meer, S., Drury, M.R., De Bresser, J.H.P., Pennock, G.M. (Eds.), Deformation Mechanisms, Rheology and Tectonics: Current Status and Future Perspectives. Geological Society, London, pp. 171–190. Special Publications, 200.
Strachan, R.A., Smith, M., Harris, A.L., Fettes, D.J., 2002. The northern Highland and Grampian terranes. In: Trewin, N.H. (Ed.), The Geology of Scotland. The Geological Society, London, pp. 81–147.
Strine, M., Mitra, G., 2004. Preliminary kinematic data from a salient-recess pair along the Moine thrust, northwest Scotland. In: Sussman, A.J., Weil, A.B. (Eds.), Orogenic Curvature: Integrating Paleomagnetic and Structural Analyses. Geological Society of America, pp. 87–107. Special Paper, 383.
Strine, M., Wojtal, S., 2004. Evidence for non-plane strain flattening along the Moine thrust, Loch Strath nan Aisinnin, northwest Scotland. Journal of Structural Geology 26, 1755–1772.
Sullivan, W.A., 2008. Significance of transport-parallel strain variations in part of the Raft River shear zone, Raft River Mountains, Utah, USA. Journal of Structural Geology 30, 138–158.
Thigpen, J.R., 2009. Regional Variation in Strain and Vorticity within Mylonites from the Moine Thrust Zone of NW Scotland. PhD thesis, Virginia Tech.
Thigpen, J.R., Law, R.D., Lloyd, G.E., Brown, S.J., Cook, B., 2010. Deformation temperatures, vorticity of flow and strain symmetry in the Loch Eriboll mylonites, NW Scotland: implications for kinematic and structural evolution of the northernmost Moine thrust zone. In: Law, R.D., Butler, R.W.H., Holdsworth, R., Krabbendam, M. & Strachan, R. (Eds), Continental Tectonics and Mountain Building – The Legacy of Peach and Horne. Geological Society, London, Special Publications 335. 623–662.
Tikoff, B., Fossen, H., 1995. The limitations of three-dimensional kinematic vorticity analysis. Journal of Structural Geology 17, 1771–1784.
Tullis, J.A., Christie, J.M., Griggs, D.T., 1973. Microstructures and preferred orientations of experimentally deformed quartzites. Geological Society of America Bulletin 84, 297–314.
Vance, D., Strachan, R.A., Jones, K.A., 1998. Extensional versus compressional settings for metamorphism: garnet chronometry and pressure-temperature-time histories in the Moine Supergroup, northwest Scotland. Geology 26, 927–930.
Vannay, J.-C., Grasemann, B., 2001. Himalayan inverted metamorphism and syn-convergence extension as a consequence of a general shear extrusion. Geological Magazine 138, 253–276.
Wallis, S.R., Platt, J.P., Knott, S.D., 1993. Recognition of syn-convergence extension in accretionary wedges with examples from the Calabrian Arc and the Eastern Alps. American Journal of Science 293, 463–495.
Willett, S., Beaumont, C., Fullsack, P., 1993. Mechanical model for the tectonics of doubly vergent compressional orogens. Geology 21, 371–374.
Williams, P.F., Jiang, D., Lin, S., 2006. Interpretation of deformation fabrics of infrastructure zone rocks in the context of channel flow and other tectonic models. In: Law, R.D., Searle, M.P., Godin, L. (Eds.), Channel Flow, Ductile Extrusion and Exhumation in Continental Collision Zones. Geological Society London, pp. 221–236. Special Publications 268.
Williams, P.F., Jiang, D., 2006. An investigation of lower crustal deformation: evidence for channel flow and its implications for tectonics and structural studies. Journal of Structural Geology 27, 1486–1504.
Xypolias, P., Spanos, D., Chatzaras, V., Kokkalas, S., Koukouvelas, I., 2010. Vorticity of flow in ductile thrust zones: examples from the Attico-Cycladic Massif (Internal Hellenides, Greece). In: Law, R.D., Butler, R.W.H., Holdsworth, R., Krabbendam, M., Strachan, R. (Eds), Continental Tectonics and Mountain Building – The Legacy of Peach and Horne. Geological Society, London, Special Publications 335, 687–714.
Xypolias, P., Kokkalas, S., 2006. Heterogenous ductile deformation along a mid-crustal extruding shear zone: an example from the External Hellenides (Greece). In: Law, R.D., Searle, M.P., Godin, L. (Eds.), Channel Flow, Ductile Extrusion and Exhumation in Continental Collision Zones. Geological Society London, pp. 497–516. Special Publications 268.